Development of a high-throughput optical assay for functional connectivity in neuron network cultures

Tompoš, Tea

University of Zagreb
Faculty of Science
Department of Biology

Tea Tompoš

Development of a high-throughput optical assay for functional connectivity in neuronal network cultures

Master thesis

Zagreb, 2022.

Sveučilište u Zagrebu
Prirodoslovno-matematički fakultet
Biološki odsjek

Tea Tompoš

Razvoj visoko-propusne optičke metode za određivanje funkcionalne povezanosti mreže živčanih stanica u kulturi

Diplomski rad

Zagreb, 2022

This thesis was conducted at the Department of Functional Genomics, Center for Neurogenomics and Cognitive Research (CNCR), Vrije Universiteit (VU) Amsterdam under supervision of Associate Professor Dr. Ruud F. G. Toonen and co-supervision of Professor Dr. Dubravka Hranilović. The thesis was submitted for evaluation to the Department of Biology, Faculty of Science, University of Zagreb, for the purpose of obtaining a master's degree in Experimental biology.

To my parents and brother.

BASIC DOCUMENTATION CARD

University of Zagreb
Faculty of Science
Department of Biology

Master thesis

Development of a high-throughput optical assay for functional connectivity in neuronal network cultures

Tea Tompoš

Rooseveltov trg 6, 10000 Zagreb, Croatia

Neurons connect into networks via synapses which are plastic and stochastic; however, all under the control of perfectly coordinated molecular machinery which facilitates synaptic coupling and communication. Any change to the presynaptic apparatus jeopardizes vesicle release, thus instantaneously altering neuronal activation. Failed or over- activation of neurons directly changes patterns of functional connectivity in the neural network, whose emergence is still a big neuroscientific mystery. For that reason, studying synaptic activity is essential for understanding functional connectivity. Many optical tools are available for probing network-wide dynamics, but little achieve single-synaptic resolution. I used a novel intensity-based glutamate-sensing fluorescence reporter (iGluSnFR) to explore its potential to report single-synaptic activity *in vitro*. iGluSnFR successfully reported evoked and spontaneous synaptic glutamate release. It also detected subtle differences in genetically modified synaptic activity when compared to wild-type. Therefore, it proved equipped to resolve many synapse-related questions. If applied in large-scale network research, iGluSnFR will contribute to better understanding of physiological and pathological changes in neural networks.

Keywords: iGluSnFR, synapse, glutamate, optical reporter, fluorescence imaging
(63 pages, 11 figures, 0 tables, 111 references, original in: English)
Thesis is deposited in Central Biological Library.

Mentor: Assoc. Prof. Ruud F. G. Toonen, PhD
Co-mentor: Prof. Dubravka Hranilović, PhD

Reviewers:
Prof. Dubravka Hranilović, PhD
Sr. lect. Julija Erhardt, PhD
Assist. prof. Sandra Hudina, PhD

Thesis accepted: 8th September 2022

TEMELJNA DOKUMENTACIJSKA KARTICA

Sveučilište u Zagrebu
Prirodoslovno-matematički fakultet
Biološki odsjek Diplomski rad

Razvoj visoko-propusne optičke metode za određivanje funkcionalne povezanosti mreže živčanih stanica u kulturi

Tea Tompoš

Rooseveltov trg 6, 10000 Zagreb, Hrvatska

Neuroni se udružuju u mreže putem sinapsi čija je aktivnost, iako promjenjiva i nepredvidiva, pod kontrolom koordiniranih molekularnih procesa koji olakšavaju sinaptičko povezivanje i komunikaciju. Svaka promjena u djelovanju presinaptičkih molekula ugrožava kontrolirano oslobađanje vezikula, što odmah utječe na daljnju aktivaciju neurona. Neispravna ili pretjerana aktivacija neurona izravno mijenja obrasce funkcionalne povezanosti u neuronskoj mreži. Nastanak tih obrazaca još je uvijek velika nepoznanica u neuroznanosti. Iz tog je razloga proučavanje sinaptičke aktivnosti ključno za razumijevanje funkcionalne povezanosti neurona u mreži. Postoje mnogi optički alati za ispitivanje aktivacije neurona u mreži, ali malo ih postiže rezoluciju pojedinačnih sinapsi. U ovom je radu korišten novi fluorescentni reporter iGluSnFR (eng. *intensity-based glutamate-sensing fluorescence reporter*) pri čemu je istraživan njegov potencijal za mjerenje aktivnosti pojedinačnih sinapsi *in vitro*. iGluSnFR je pokazao efikasnost u mjerenju presinaptičkog glutamata oslobođenog nakon stimulacije ili spontane sinaptičke aktivnosti. Također, iGluSnFR je otkrio suptilne razlike u genetski modificiranoj sinaptičkoj aktivnosti u usporedbi s divljim tipom. Stoga se iGluSnFR pokazao učinkovitim za rješavanje mnogih pitanja vezanih uz sinaptičku aktivnost. Primjena iGluSnFR reportera u istraživanju neuronskih mreža pridonijet će boljem razumijevanju njihovih fizioloških i patoloških promjena.

Ključne riječi: iGluSnFR, sinapsa, glutamat, optički reporter, fluorescencijska mikroskopija
(63 stranica, 11 slika, 0 tablica, 111 literaturnih navoda, jezik izvornika: engleski)
Rad je pohranjen u Središnjoj biološkoj knjižnici

Mentor: Izv. prof. dr. sc. Ruud F. G. Toonen
Komentor: Prof. dr. sc. Dubravka Hranilović

Ocjenitelji:
Prof. dr. sc. Dubravka Hranilović
V. pred. dr. sc. Julija Erhardt
Doc. dr. sc. Sandra Hudina

Rad prihvaćen: 8. rujna 2022.

TABLE OF CONTENTS

ABBREVIATIONS

AP	Action potential
EPSP/IPSP	Excitatory/inhibitory postsynaptic potential
SV	Synaptic vesicle
NT	Neurotransmitter
iGluSnFR	Intensity-based glutamate-sensing fluorescent reporter
TTX	tetrodotoxin
WT	Wild-type
Tomosyn$^{-/-}$	Tomosyn double knockout
F	Fluorescence
F_0	Baseline fluorescence
mGT	Miniature glutamate transient
RRP	Readily-releasable pool

1. INTRODUCTION

1.1. Functional connectivity in neuronal networks

To accomplish a given task, complex systems tend to have a central organizing unit that processes information and sends appropriate commands to its acting parts. Human body can be classified as a complex system. The central unit which integrates relevant information and resultantly orchestrates human behavior is the brain. Anatomical studies of the brain point to the cerebral cortex, the outermost layer of the brain, as its executive part. This function is carried out by billions of cells called neurons (**Purves et al.**, **2008**). Individual neurons perform neurobiological computations to transform input to output information (**Koch & Segev**, **2000**). Based on the type of computations they specialize in, cortical neurons allow division of the cortex into three broad functional areas. First, there are sensory areas which contain neurons that process various types of sensory inputs (e.g., visual, auditory, tactile). Second, neurons in the association areas perceive the sensory information by assigning context to it and, if needed, store it in long-term memory. The two areas in turn send signals to the third, motor areas whose neurons generate precise commands for the body to act (**Marieb & Hoehn**, **2015**). Neurons therefore constitute brain regions that are task-specific, and their activation seems highly ordered.

However, detailed exploration of single-cell properties show a somewhat disordered picture. Rather than being deterministic in nature, neuronal response to the incoming stimuli is surprisingly probabilistic. For instance, principally tuned neurons in the primary sensory cortex of rats respond to whisker stimulation on the animal's snout (**Celikel et al.**, **2004**). Yet, a closer look into single-cell activation patterns shows that these neurons on average have 0.5 activation probability upon stimulation, and they show activity rates < 1 Hz (**Kerr et al.**, **2007**; **Ranjbar-Slamloo & Arabzadeh**, **2019**). It is therefore thought that the stimulus-specific response of individual neurons is unreliable and, as such, insufficient for downstream regions to decode the ongoing activity (**K. D. Harris**, **2005**; **Yuste**, **2015**). So, the relationship between single neuron activity and stimulus representation is nontrivial and is still being widely explored (**Adibi**, **2019**; **Benedetti et al.**, **2009**). An emerging hypothesis suggests that stimulus representation happens on a population level, so presumably the greatest potential of neurons is achieved when

connected with others in so-called neural (or neuronal) networks (**Buzsáki**, **2010**). Indeed, storing stimulus features in population activity grants downstream areas to decode with increased reliability (**Barrett et al.**, **2016**; **Dubreuil et al.**, **2022**).

Neural networks are formed from anatomical contacts between neuronal processes. Since most cortical neurons belonging to a local brain region have short-ranging and overlapping processes, it is expected that neighboring neurons form anatomical networks, and therefore get activated all together during stimulus representation. However, probing neural network activity revealed a significant amount of trial-to-trial variability in population response to identical stimuli (**Cui et al.**, **2016**; **Dinstein et al.**, **2015**; **Fontanini & Katz**, **2008**). These results show that anatomically connected networks do not engage in identical activity patterns despite the unchanged experimental conditions. In other words, not all neurons in the local network will respond to the repeated stimulus. Interestingly, this variability does not affect the downstream decoder, so the stimulus-triggered behavior remains constant (**Cui et al.**, **2016**). Varying activity patterns make it apparent that the same stimulus can be represented by activating different constellations of neurons in an anatomically connected network, possibly depending on the network's previous state (**Fontanini & Katz**, **2008**). Hence, neural networks display a second order connectivity called functional connectivity. It is defined by temporal correlation in single-cell activity and it superimposes hard-wired anatomical connections.

Functional networks have indisputable advantages over the anatomical ones. Both are known to undergo activity-dependent dynamic changes known as network plasticity; however, to a substantially different degree. For instance, a functional network exerts a rapid reconfiguration ability that occurs within seconds or less. Meanwhile, structural changes in anatomical connectivity (i.e. re-wiring of the same network) take from dozens of minutes to hours (**Bullmore & Sporns**, **2009**). One can imagine that transient, instantaneous change in the pattern of functional connectivity is an asset for the brain. This operational mode can be utilized during highly demanding cognitive exercises like the working memory task, where different neural assemblies are used for short-term mnemonic purposes (**O'Reilly**, **2006**).

It is necessary to understand the principles of functional networks formation from the underlying anatomical connectivity. Firstly, because connectivity fundamentally controls the information transfer in the network (**Huang et al.**, **2020**; **Laughlin & Sejnowski**, **2003**). Yet, what are the rules of information transfer at the network level, and how does the activation of

different functional ensembles affect those rules, remains largely unknown. Secondly, hallmarks of many neuropathologies include anatomical or functional changes to neural networks. For instance, in neurodegenerative diseases like Alzheimer's disease (AD), anatomical connectivity is either affected quantitatively through cell loss or qualitatively by the loss of plasticity (**Andrade-Talavera & Rodríguez-Moreno**, **2021**). Moreover, in cases like epileptic encephalopathy (EE), there are mutations in genes encoding proteins that are central for information transmission in the network, thus affecting its functionality while connectivity stays intact (**Saitsu et al.**, **2008**; **Stamberger et al.**, **2016**). Severity of behavioral symptoms in AD and EE patients suggests that the crucial aspects of neural network activity are highly compromised in both cases. So, studying functional connectivity in diseased networks will yield answers we miss while trying to understand brain pathologies.

Fitting methodology is critical in revealing answers to questions related to neural network properties. Currently available tools for functional network connectivity research do not offer sufficient spatial resolution. Those are suitable to study connectivity among large-scale networks of distant brain regions with great power, like functional magnetic resonance imaging (fMRI) and electroencephalography (EEG) (**Eickhoff & Müller**, **2015**; **Rossini et al.**, **2019**), but they remain clueless to cell-specific activity in local neural networks. That is, for instance, why the full extent of functional consequences caused by AD, EE and other changes in local network connectivity cannot be assessed. These methodological shortcomings serve as principal motivation for this work.

1.2. Synapse as a functional unit in neural networks

Neurons are functionally polarized cells – they have extensively branched filaments growing out of their bodies that specialize in sending information on one end, and receiving information on the other. Former are known as axons and latter as dendrites. The first out of two main developmental mechanisms in neural network formation involves extension of axons and dendrites in search of binding partners (**Purves et al.**, **2008**). Once a neuron's axonal segment reaches the critical proximity to another neuron's dendrite or soma, the second mechanism will onset. It concerns the formation of specialized anatomical structures called synapses (**Figure 1a**). The synapse is a unique structure of vast molecular complexity that mediates neuronal communication at the level of axodendritic or axosomatic contacts.

Molecular interactions in mature synapses facilitate translation of presynaptic electrical impulses, known as action potentials (APs or spikes), into a chemical signal that traverses across the synaptic cleft, and again triggers electrical changes in the postsynaptic membrane that will eventually make the postsynaptic neuron spike. Thus, synaptic activity allowing AP propagation from pre- to postsynaptic neurons is a step essential to information transfer in the network. An intriguing result was obtained in a study which explored the consequences that synaptic activity removal had on animal behavior (**Verhage et al., 2000**). They showed that neural networks are formed unaffectedly in the absence of synaptic activity during gestation in animals with genetically silenced synapses. However, these animals die immediately upon birth due to rapid neuronal cell death caused by a complete lack of synaptic transmission. Verhage et al. (**2000**) clearly revealed the importance of synapses for neural network functioning. They turned the focus on synaptic activity-related questions while studying neural networks.

Different synaptic properties were uncovered which have shown that not all synapses are functionally unique across a neural network. The main indicator of so-called synaptic efficacy is the relative synaptic strength. It is commonly described by measuring the amplitude of postsynaptic potential (PSP) as a response to presynaptic AP. Change in synaptic strength is activity-dependent, whereby salient stimuli tend to reactivate the same synapses which increases their strength, and disappearing stimuli lessen synaptic efficacy due to synapses being unused (**Allen et al., 2003**; **Celikel et al., 2004**; **Gambino et al., 2014**, **Aroniadou-Anderjaska & Keller, 1995**; **Malenka, 1995**; **Malenka & Bear, 2004**; **Mu & Poo, 2006**). Activity-dependent modulation of synaptic efficacy is also known as activity-dependent plasticity. Synapses show short- and long-term plasticity (STP and LTP, respectively) which are defined by the timescale at which activity-induced changes persist in synapse. STP will result in instantaneous changes that return to baseline synaptic functioning in minutes, whereas LTP results in long-lasting changes (hours, days and more) (**Citri & Malenka, 2008**). Out of the two, short-term plasticity directly alters computations in functional networks via transient facilitation and depression of synaptic activity (**Barroso-Flores et al., 2017**; **Hennig, 2013**; **Jaaskelainen et al., 2011**).

All synapses are prone to activity-dependent changes. Therefore, presynaptic inputs to a neuron vary in strengths and signs, where the latter depends on whether it comes from excitatory or inhibitory synapse (**Figure 1b**). Inputs from spatially distributed synapses along

the neuronal dendritic tree are in turn integrated at somatic level by means of spatial summation (**Figure 1c**). It results in membrane potential fluctuations around the axonal initial segment where, if fluctuation crosses the spiking threshold, a postsynaptic neuron will generate an AP. This relationship between single-synaptic activity and neuronal firing is among central focuses while explaining functional activation of neurons in neural networks. To understand how different synaptic activity regimes arise, it is first necessary to consider a sequence of physiological steps involved in a single synaptic activity cycle.

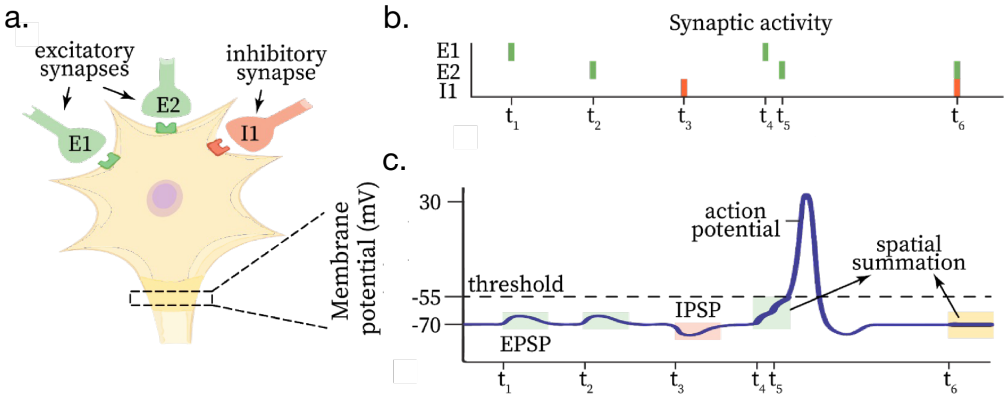

Figure 1. Presynaptic activity and postsynaptic neuronal response. (a) Two excitatory (E1, E2) and one inhibitory (I1) synapses converge onto a postsynaptic neuron (beige). **(b)** Raster plot of corresponding synaptic activity. Every line marks the time of each synaptic spike. **(c)** Membrane potential change at the axon hillock. EPSP, excitatory postsynaptic potential; IPSP, inhibitory postsynaptic potential. Adapted from (*Spinal Reflex Electrophysiology*, n.d.).

1.2.1. Central events leading to synaptic transmission

Neural communication is spatially and temporally precise and the direction of information flow goes from the presynaptic to the postsynaptic cell. These constrictions require specialized molecular machinery whose acting parts will reliably and repeatedly interact to ensure successful synaptic transmission. Two synapsing neurons connect via the active zone (AZ) on the presynaptic side and the postsynaptic density (PSD) on the postsynaptic side. Mutual recognition and alignment of AZ and PSD are governed by the synaptic cell adhesion molecules (SCAMs). They assure tight trans-synaptic interactions, but leave a crucial part of

the intercellular space, known as synaptic cleft, open for neurons to exchange molecular material (**Missler et al.**, **2012**). One significantly important class of molecules that crosses the cleft are neurotransmitters (NTs). They are associated with AP-encoded information transfer in neural networks and are divided in three categories – excitatory, inhibitory and neuromodulatory NTs (**Purves et al.**, **2008**). NTs are stored in presynaptic organelles called synaptic vesicles (SV) prior to their release into synaptic cleft.

SVs are fundamental to every presynapse, therefore presynaptic activity can be understood by closely examining the synaptic vesicle cycle (**Figure 2a**) and the roles of proteins involved therein (see **1.1.3.; Figure 2b**). First, NTs are packed in synaptic vesicles in a process actively mediated by a group of SV-related transport proteins. Once SVs are loaded (**Figure 2a, step (1)**), they are being guided by a group of SV trafficking proteins to the presynaptic release site (**Südhof**, **1995**). They cluster near the AZ, where only a few of them are docked at the AZ plasma membrane at a time (**Figure 2a, step (2); Becherer & Rettig**, **2006**). Docking represents the initial contact between the SV and plasma membrane. It is followed by the vesicle priming, which includes additional immobilization of the SV (**Figure 2a, step (3); Südhof**, **2012**). Primed SVs are release-ready and form a so-called readily releasable pool (RRP; **Becherer & Rettig**, **2006**). When AP reaches the presynaptic terminal, it causes a sudden change in electric potential difference across the presynaptic membrane. This triggers opening of the voltage-gated calcium (Ca^{2+}) channels (VGCCs) which are sensitive to changes in membrane potentials, causing a sudden rise in intracellular Ca^{2+} concentration (**Südhof**, **2004**; **Südhof & Rizo**, **2011**). The interaction between Ca^{2+} and SV fusion machinery eventually leads to vesicle exocytosis and the release of NTs into the cleft (**Figure 2a, step (4)**; see section below). The vesicular membrane is endocytosed outside of the AZ in perisynaptic space and is recycled in few additional steps before the next neurotransmitter uptake event onsets (**Figure 2a, steps (5a-c)**; **Saheki & De Camilli**, **2012**).

Synaptic cycle continues on the postsynaptic side and it depends on the neurotransmitters' effect. Different NTs show reactivity with specific postsynaptically expressed receptors (**K. M. Harris & Weinberg**, **2012**). A class of ionotropic NT receptors includes transmembrane channels with ion-specific permeability. Hence, their opening will have differential effects on the postsynaptic membrane potential (PSP) change. For instance, the main excitatory neurotransmitter glutamate will bind to ionotropic receptors that are non-

selectively permeable to monovalent cations, namely sodium (Na^+) and potassium (K^+), but selectively to Ca^{2+} (**Ottersen & Landsend**, **1997**; **Wollmuth**, **2018**). At baseline membrane potential of around -65 mV, fast Na^+ influx through the channel's pore will depolarize the postsynaptic membrane to cause excitatory PSP (EPSP; **Figure 1c**). EPSP brings the cell closer to the critical point of crossing the spiking threshold, which is on average around -55 mV; however, it is highly adaptive (**Wilent & Contreras**, **2005**). Conversely, the main inhibitory neurotransmitter GABA (γ-aminobutyric acid) binds ionotropic receptors which are permeable to chloride (Cl^-) and bicarbonate (HCO_3^-) ions (**Farrant & Nusser**, **2005**). Their influx into postsynapse hyperpolarizes the membrane to cause inhibitory PSP (IPSP; **Figure 1c**). IPSP shifts the membrane potential further away from the spiking threshold of a postsynaptic neuron. As discussed in the previous chapter, dendritic EPSPs and IPSPs are integrated at the level of soma by the rule of spatial summation to eventually generate AP.

Both pre- and postsynaptic events are largely important for shaping activity of neural networks. However, the postsynapse is usually associated with LTP-related mechanisms which induce structural modifications to synapse (**Gambino et al.**, **2014**; **Kennedy**, **2000**). Long-lasting changes in synaptic structure may affect functional connectivity, but indirectly and on a slower timescale. The two mechanisms directly implicated in influencing functional connectivity are the NT release and its modulation through STP (**Südhof**, **2012**). These are presynapse-specific mechanisms, therefore, functional connectivity is better studied from the presynaptic perspective. Successful research into presynapse requires understanding its molecular structure. Therefore, the next chapter addresses crucial protein-protein interactions which mediate presynaptic functioning described above.

1.2.2. Critical presynaptic machinery for proper synaptic vesicle secretion

Extensive research targeting presynaptic proteins has uncovered many essential protein-protein interactions required for successful synaptic transmission. Two big protein complexes mediate SV docking, priming and fusion/exocytosis. One is composed of the active zone proteins, hence titled the active zone complex (**Südhof**, **2012**), and the other is known as the core fusion complex due to its central role in SV fusion (**Figure 2b;** (**Südhof**, **2012**; **Südhof & Rizo**, **2011**). The active zone complex has a suggested role in SV docking and priming during which it enables the co-localization of SVs with the VGCCs (**Emperador-Melero & Kaeser**, **2020**). This event is of great importance for fast excitation-release coupling. There are

seven evolutionarily conserved proteins known to form the active zone complex: RIMs (from Rab3-interacting molecules), RIM-BPs (from RIM-binding proteins), Munc13s, α-liprins, ELKS proteins, together with Bassoon and Piccolo (**Chua**, **2014**; **Emperador-Melero & Kaeser**, **2020**; **Südhof**, **2012**). Note, however, that many of them are encoded by multiple genes and exist in many isoforms (e.g. RIM1 and RIM2 genes code for RIM1α and RIM1β, and RIM2α and RIM2β, respectively (**Südhof**, **2004**)). This dramatically increases the variety of presynaptic protein composition, which is still an area of great research interest.

In a simplistic descriptive model of the mammalian secretory machinery (**Figure 2b**), the active zone complex formation begins with the activation of an inactive Munc13 homodimer by RIM. Both Munc13 and RIM proteins interact at their amino terminals. Moreover, RIM has a centrally positioned domain that binds the cytoplasmic tail of VGCCs. Their bond is further reinforced by RIM-BP, which independently binds both the VGCC's cytoplasmic tail and RIM. Additionally, RIM is known to bind ELKS, as well as α-liprin. Because VGCCs are membrane-bound, the RIM/RIM-BP/VGCC interaction links the active zone complex to the AZ plasma membrane. On the other side of the active zone complex, RIM/Munc13 segment connects to the SV membrane via RIM's interaction with SV-associated protein Rab3. This bond is crucial to docking the synaptic vesicle to the active zone by the active zone complex (**Emperador-Melero & Kaeser**, **2020**; **Südhof**, **2012**; **Südhof & Rizo**, **2011**). Vesicle docking is followed by priming, an event triggered by partial assembly of the core (fusion) complex.

As was the case with the active zone proteins, the core complex proteins occur in multiple isoforms and are evolutionarily conserved. Their absence from the presynapse completely abolishes synaptic transmission, proving they are essential for SV fusion (**Bronk et al.**, **2007**; **Toonen & Verhage**, **2007**; **Vardar et al.**, **2016**; **Verhage et al.**, **2000**). They come from the two protein families known as SNAREs (for soluble NSF-attachment protein receptors; NSF for N-ethylmaleimide sensitive factor) and SM (for Sec1/Munc18-like) proteins. Out of the three SNARE proteins, Syntaxin-1 and SNAP-25 (for synaptosomal associated protein of 25 kDa) are found in the plasma membrane, while synaptobrevin/VAMP2 (for vesicle-associated membrane protein 2) is attached to the SV membrane. Partial assembly of the core complex, hereafter the trans-SNARE complex, includes parallel positioning of two SNARE motifs from SNAP-25's structure, and one from both Syntaxin-1 and

synaptobrevin/VAMP2 in a four-helix bundle (**Figure 2b**; **Südhof & Rizo**, **2011**). Interestingly, the trans-SNARE complex formation is catalyzed by an active zone complex protein Munc13 via its MUN domain (**Südhof**, **2012**). Moreover, the trans-SNARE complex is joined by the SM protein Munc18-1/STXBP1 (for syntaxin binding protein 1). Munc18-1 is able to bind the assembled trans-SNARE complex in many modes, all of which are thought to control various aspects of presynaptic events leading to SV priming and later fusion (**Toonen & Verhage**, **2007**). It was suggested that energy released upon the trans-SNARE complex assembly induces a partial fusion pore opening via mechanical force onto the presynaptic membrane (**Südhof & Rizo**, **2011**). The formation of trans-SNARE complex concludes the priming step in the SV cycle, making the SV fusion-competent.

Primed SVs wait for a trigger before they undergo fast exocytosis-mediated fusion. The trigger comes in the form of AP-induced change in membrane potential in the presynapse. This causes opening of the VGCCs, followed by the fast Ca^{2+} influx into the AZ. However, a mere presence of Ca^{2+} is not sufficient to coordinate synchronous SV release which is necessary for temporally precise information transfer between neurons. Rather, SVs need a designated Ca^{2+} sensor to facilitate SV fusion. Research shows that the vesicular transmembrane protein Synaptotagmin-1 (Syt-1) acts in this regard (**Chapman**, **2008**; **Chua**, **2014**). Upon binding Ca^{2+} (**Figure 2b**), Syt-1 interacts with trans-SNARE complex to onset fusion pore opening which in turn prompts rapid NT release. Immediately after the fusion, the trans-SNARE complex is converted to cis-SNARE complex by ATPase NSF and its adaptor proteins (**Sudlow et al.**, **1996**; **Zhao et al.**, **2007**). Further enzymatic activity of NSF results in dissociation of cis-SNARE complex (**Südhof & Rizo**, **2011**). This marks the start of local recycling of SNARE/SM proteins for their reuse in the next SV cycle.

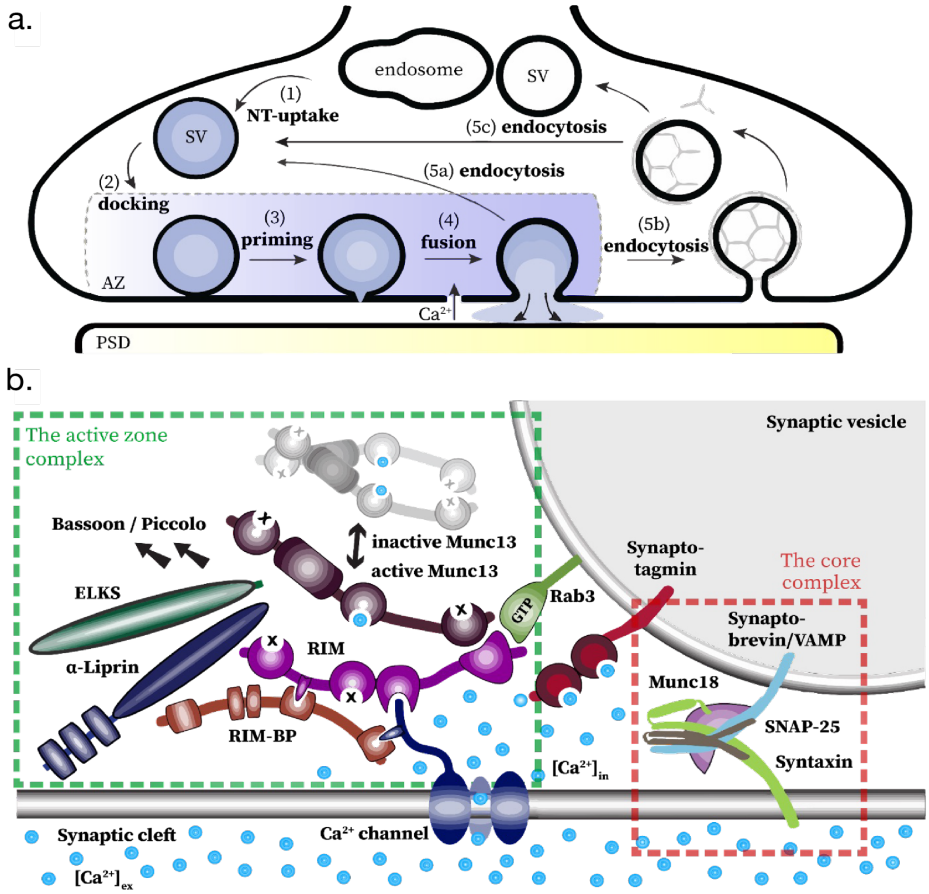

Figure 2. The synaptic vesicle (SV) cycle and its essential regulatory machinery. **(a)** Synaptic vesicle cycle leads to neurotransmitter release into the synaptic cleft. Ca^{2+}, calcium ions; AZ, active zone; PSD, postsynaptic density. Adopted from (**Chua**, **2014**). **(b)** Two protein complexes, the active zone complex and core complex, and their accessory proteins essential for SV docking and fusion. Adapted from (**Südhof**, **2012**).

As described above, the active zone complex and the trans-SNARE complex are accompanied by key accessory proteins (Rab3, Munc18-1, Syt-1) that promote timely and synchronous SV release. However, regulation of synaptic vesicle cycle requires proteins that have negative control over SV release to achieve tight and balanced synaptic activity. Experiments have shown that Tomosyn/STXBP5 (for syntaxin binding protein 5) inhibits synaptic transmission by reducing the availability of release-ready SVs (**Cazares et al.**, **2016**; **Gracheva et al.**, **2006**; **McEwen et al.**, **2006**; **Park et al.**, **2017**; **Yizhar & Ashery**, **2008**). Current data point to three putative mechanisms of Tomosyn's action. It binds Syntaxin and SNAP-25 to form non-fusogenic SNARE complexes which (1) prevent the immobilization of

newly arriving vesicles to the active zone, and (2) attenuate immobilization of already docked SVs (**Ashery et al.**, **2009**; **Yizhar & Ashery**, **2008**). Post-fusion, Tomosyn is also able to (3) oligomerize cis-SNARE complexes, thus decreasing the amount of available SNARE proteins for the next fusion cycle (**Ashery et al.**, **2009**). Altogether, promoters and inhibitors of vesicular release work in concert to modulate vesicle release probability. They are directly responsible for initially introduced stochasticity of neuronal activation that underlies functional connectivity. Many unanswered questions still wait to be addressed, some of which were on hold due to missing technology. Next chapter reviews fitting methodological approaches to study synaptic activity in functional connectivity context.

1.3. Electrophysiological *versus* optical approach to neural recordings

Neurons have intrinsic physiological properties and functions that lead to their activation. They are electrically excitable cells, so physiological properties can be revealed by monitoring electrical signals associated with their activity as they respond to stimuli in real-time. Many tools have been developed for recording electrical signals from the brain. The standard experimental approach is to directly measure membrane potential of individual cells. Most commonly used method for direct access into intracellular electrophysiological properties is known as patch-clamp method (**Liem et al.**, **1995**). A whole-cell implementation of patch-clamp recording gives insight into the intracellular signal using a glass micropipette containing a recording electrode. Micropipette penetrates the neuronal cell body to establish a tight seal between the cell membrane and internal solution contained in the micropipette. Internal solution mimics cell contents, thus any change to it caused by membrane depolarization in a recorded neuron will be detected by an electrode immersed in the solution.

Patch-clamp method has many advantages. It is extremely sensitive, so even the slightest neuronal activity will be recorded. It directly records the voltage signal from neuronal soma which eases signal interpretation and analysis. The tight seal between micropipette and somatic membrane grants fast signal acquisition and high signal-to-noise (SNR) ratio. Former is needed to reliably track neuronal firing rates across time, and latter to easily detect AP events from the noisy signal. Patch-clamp is necessarily combined with microscopy to visualize micropipette while it advances through neural tissue to establish the seal with neuronal membrane. Microscopic imaging allows cell identification which is important for locating

neurons in the brain and interpreting their function. However, there are certain drawbacks related to the patch-clamp approach. Because it involves external tools penetrating brain tissue, physical constraints of its instrumentation prohibit multi-neuronal experimental designs. Only a limited number of micropipettes controlled by externally positioned micromanipulators fit under the experimental setup. The upper limit of simultaneously patched neurons achieved on average is 4, while only rarely multi-neuron patch-clamp experiments successfully involve more cells, with maximum being around 10 (**Peng et al.**, **2019**). Furthermore, how micropipette reaches neuronal soma is highly invasive and it causes damage both to the patched neuron and surrounding tissue. Patching a neuron, therefore, leaves a short window of time for experimental recording before the cell dies due to stress, usually after an hour. So, the method's precision and speed in signal acquisition is secondary when patch-clamp is considered in the context of neural network research. In that case, the number of neurons accessible to record from is priority.

There are other powerful electrophysiological methods commonly used that are well suited for network studies. For example, multi-electrode arrays (MEAs) record activity from hundreds of neurons in the network (**Marre et al.**, **2012**). MEAs likewise have fast temporal resolution during signal acquisition, and they access voltage signals coming from local networks. However, MEAs and similar devices contain sensors which are placed in the vicinity of neuronal bodies and target certain brain regions rather than individual cells. Therefore, instead of intracellular activity, multi-electrode devices record extracellular change in field potential to which many surrounding neurons contribute. This is an unfavorable property of multi-electrode approaches since both single-cell precision and identity of individual neurons are lost. Thus, the most powerful electrophysiological approaches for single- and multi-neuron research fail in two crucial requirements to be able to analyze functional network connectivity. First, neurons need to be recorded in great numbers and second, their identity must be tracked throughout recording.

Continuous expansion of knowledge about molecular organization of neurons points to several opportunities to develop better technologies for monitoring neuronal activity in networks (**Shen et al.**, **2020**). These technologies leap from electrophysiology to a completely new field of optical methods. Most widely used optical method is calcium imaging. In general, calcium influx into cytosol resulting from AP-triggered membrane depolarization was

leveraged to approximate neuronal activity while preserving cell identity in the network (**Ali & Kwan**, **2019**). Theoretical aspect of this approach is as follows. Since intracellular concentration of calcium ($[Ca^{2+}]_{in}$) prior to AP generation is low, detecting a transient peak in $[Ca^{2+}]_{in}$ rise is indicative of recent neuronal activity. Researchers have engineered molecular probes with high Ca^{2+} sensitivity that are structurally coupled with various fluorescence-emitting proteins (FPs or fluorophores) (**Shen et al.**, **2020**; **Tian et al.**, **2012**). Calcium probe is then expressed in neurons whose activity is wished to be monitored. Native conformation of the probe is a calcium-unbound state in which the fluorophore is quenched i.e., unable to emit fluorescence. Although, there is a substantial amount of baseline fluorescent light being spontaneously emitted when neurons are at rest due to stochastic properties of the probe. Binding Ca^{2+} ions during increased cytosolic Ca^{2+} levels leads to a conformational change in part of the probe's structure containing the fluorophore. This causes de-quenching of the fluorophore. Consequently, the result is a transient peak in the signal amplitude due to increased fluorescence emission, thus reflecting the timing of AP during neural activity.

Calcium-sensitive probes differ from electrophysiological methods in that they do not report neuronal activity in the form of electrical, but as optical signals. Optical experiments rely on fluorescence microscopy techniques rather than on arrays of electrodes or micropipettes (**Broussard et al.**, **2014**; **Grienberger & Konnerth**, **2012**). Every probe is defined by the excitation and emission light whose wavelengths are spectrally separated. Excitation light is used to continuously illuminate the probe throughout the experiment. It gets absorbed by the fluorophore and converted into emission light when fluorophore is de-quenched. Every optical experimental setup contains a set of wavelength-specific filters which block excitation light from entering the imaging sensor, but they pass emission light through. That way, optical recordings contain continuous images of neurons whose activity is captured by the emission of fluorescent light coming from activated probes. Good optical recordings have sharply filtered emission light, fast image acquisition rate, and optical probes producing high SNR and showing fast kinetics.

The unprecedented advantage of optical approach over electrophysiology is that it gives insight into neuronal activity with intracellular resolution while preserving the cell identity. As opposed to electrophysiological techniques, optical tools are non-invasive, so they allow for continuous research over hours, days and weeks (**Razlivanov et al.**, **2018**; **Sadakane et al.**,

2015). When a fluorescent probe is present in neurons across the population, results obtained by continuously imaging population activity consist of precise locations and signal traces from individual neurons. Therefore, optical tools assure high-throughput data acquisition which is out of reach for many other techniques. As such, they are ideally suitable for functional network studies.

1.3.1. Optical tools for detection of presynaptic activity

Functional network connectivity relies on synaptic transmission which is modulated by short-term plasticity and change in NT release probability, both of which are presynaptic phenomena (see Chapter 1.1.2.). Therefore, for optical interrogation of functional networks, it is preferable to achieve single-synaptic resolution. So far, optical reporters designed to sense the change in $[Ca^{2+}]_{in}$ are currently most used probes for fluorescence imaging. They revolutionized neural network research in many ways. A group of genetically encoded calcium indicators (GECIs; **Grienberger & Konnerth, 2012**; **Tian et al., 2012**) allowed a non-invasive and genetically targeted expression in neurons of specific types and brain locations. In addition, genetic targeting avoids reporter expression by non-neuronal cells like astrocytes. It also eliminates the issue of residual extracellular fluorescence specific for bulk loading of previously dominant synthetic Ca^{2+} reporters or dyes (**Broussard et al.**, **2014**; **Grienberger & Konnerth**, **2012**). This in turn significantly reduces background fluorescence that threatens to dampen AP signals by decreasing SNR.

The GCaMP family of GECIs became a standard tool in optical neurophysiology performed both *in vivo* and *in vitro* (**Broussard et al.**, **2014**). They continuously improve in performance by the means of protein engineering, so that recent iterations named GCaMP6 (**T.-W. Chen et al.**, **2013**), jGCaMP7 (**Dana et al.**, **2019**) and most recently jGCaMP8 (**Zhang et al.**, **2020**) have progressively higher SNR, faster kinetics and stronger expression levels among other essential properties. Interrogations of networks using GECIs have revealed results previously inaccessible through electrophysiological approaches (**Keller et al.**, **2020**). Most GECIs including GCaMPs are equally distributed throughout cytosol expressed in neurons. This, however, makes it difficult to locate activity coming from single synapses along the neurites, and requires additional expression of a presynapse-specific molecular label for *post hoc* image analysis. Even then, GECIs have slow kinetics relative to millisecond-short fluctuations in membrane potential in single synapses. That makes isolating individual

presynaptic activity hardly possible when analyzing somatic calcium traces. Alternatively, GECIs can be fused to presynaptic proteins for targeted localization to the presynaptic compartment (**Dreosti et al.**, **2009**). This approach will avoid signal contamination by somatic Ca^{2+} increase, since the probe then reflects only the increase in $[Ca^{2+}]_{in}$ at presynaptic terminals. Still, some concerns remain. As described earlier, GECIs detect changes in cytosolic $[Ca^{2+}]_{in}$ dynamics, but those act as a proxy of AP generation rather than directly reflecting membrane potential change. This approximative property raises questions linked to (non-)linear relationship between synaptic activity and calcium dynamics during signal interpretation (**Jackson & Burrone**, **2016**). To overcome these constraints, optical reporter engineering has focused on presynapse-specific events (see Chapter 1.1.2.) and molecules (see Chapter 1.1.3.) to design probes that undoubtedly report the activity of single synapses (**Dreosti & Lagnado**, **2011**).

There are two target events significant for synaptic transmission that proved particularly successful for optical reporter design. Those are (1) SV fusion with the presynaptic cell membrane and (2) NT release into the synaptic cleft. Prior to fusion, SV lumen is maintained at the slightly acidic pH of ~ 5.6. Upon fusion, the pore opening causes mixing of SV ionic content with the extracellular environment whose pH is neutral (~ 7.4). Therefore, for a brief moment before the SV endocytosis and re-acidification occur, vesicular lumen neutralizes in pH. This mechanism was utilized to create pH-sensitive probes that report neural activity based on AP-triggered SV fusion/exocytosis (**Jang et al.**, **2021**). Most widely used are pH-sensitive green fluorescent protein (GFP)-based probes named pHluorins. When residing in acidic SV lumen, pHluorins are in a protonated state which keeps their fluorescence quenched. Amidst brief exposure to the neutral pH during SV fusion, pHluorins undergo deprotonation and de-quenching of GFP, thereby reporting SV fusion/exocytosis by transiently increasing fluorescence emission. Fluorescence signal decreases as endocytosed SVs get re-acidified. Despite the wide use due to their flexibility when fused to different presynaptic proteins (**Diril et al.**, **2006**; **Granseth et al.**, **2006**; **Sankaranarayanan et al.**, **2000**), pHluorins have certain limitations. Synaptic activity is reported as a fraction of released SVs instead of directly quantifying neurotransmission. Additionally, the change in pHluorin fluorescence signal is not only a function of SV exo-/endocytosis rate, but it is also affected by the rate of re-acidification of recently endocytosed vesicles. Hence, interpretation of the signal can be ambiguous.

Individual presynaptic activity is best reported using probes directly sensitive to neurotransmitters. Those will be discussed in the following section.

1.3.2. Genetically encoded neurotransmitter reporters (GETIs)

The quest for optical monitoring of neurotransmission culminated with the development of genetically encoded neurotransmitter reporters (GETIs; **Shen et al., 2020**). Their advent opened a dimension previously unreachable with probes such as calcium or pH-sensitive reporters. Neurotransmission could be quantified based on the type of information communicated between synapses i.e., excitatory, inhibitory or neuromodulatory. Indeed, different GETIs were developed to quantify excitation by detecting glutamate, inhibition by detecting GABA, and detecting neuromodulation facilitated by dopamine, acetylcholine or norepinephrine (reviewed in (**Sabatini & Tian**, **2020**)). Glutamate sensitive GETIs are particularly interesting for current work. They allow studying signal transduction, presynaptic plasticity and SV release properties among other aspects of functionally connected networks. The first genetically encoded glutamate-sensing fluorescence reporter (GluSnFR) was constructed using Glt1, a periplasmic binding protein (PBP) with affinity for glutamate that is native to *Escherichia coli*. Glt1 was fused with two spectrally diverse fluorophores, namely the cyan-emitting ECFP (for enhanced cyan fluorescent protein) and yellow-emitting Citrine (**Hires et al.**, **2008**). When expressed in neurons, GluSnFR is anchored to the plasma membrane with its glutamate-binding domain exposed to the synaptic cleft. In the baseline condition i.e., when neurons are at rest, ECFP actively emits fluorescence. When glutamate is released into the synaptic cleft, it binds GluSnFR which causes conformational change in its structure. Conformational restructuring pulls the two fluorophores closer together, triggering proton transfer from ECFP to Citrine via the mechanism known as Förster resonance energy transfer (FRET). This activates yellow fluorescent light emission which has been quenched in baseline. Therefore, excitatory synaptic activity is visualized based on a ratiometric change in fluorescence between the two fluorophores.

GluSnFR was later advanced into SuperGluSnFR which exhibited better response size in terms of ratiometric change between cyan and yellow fluorescence, as well as having faster kinetics and higher SNR (**Hires et al.**, **2008**). However, these types of probes still have their limitations. FRET-based GluSnFRs occupy a large part of the optical spectra which minimizes the possibility for simultaneous multi-probe optical experiments. Furthermore, they elicit

relatively weak change in fluorescence, so averaging over more trials is necessary to detect synaptic response. A major improvement was made when a single-FP probe was engineered (**Marvin et al.**, **2013**). Fluorescence signal yielded by the new GluSnFR was intensity-based (hence the upgrade of their name, iGluSnFR), rather than FRET-based. This was achieved by fusing a circularly permuted (cp-) GFP to the already known Glt1 protein. In glutamate-unbound state, cpGFP contains two misaligned β-barrels that distort its original structure, therefore prohibiting fluorescence emission and causing low fluorescence intensity at baseline. Alignment of the β-barrels in glutamate-bound state mediates approximately 5-fold increase in cpGFP fluorescence with respect to that of SuperGluSnFR (**Marvin et al.**, **2013**). This significantly exceeded the performance of any glutamate-sensing reporter so far. As **Marvin et al.** (**2013**) report, iGluSnFR was able to resolve single APs in a train delivered at 10 Hz stimulation frequency. Its ~4 μM affinity for glutamate was suitable for reporting a range of synaptic activity strengths which varied in glutamate release load. It was applied in most common vertebrate and invertebrate animal models with great success both *in vivo* and *in vitro*. However, the signal plateaued for higher numbers of APs (20-160 APs at 30 Hz), and the probe struggled during heavy glutamate loads resulting from strong synaptic activity which would reach millimolar quantities. Additional protein engineering yielded at least two improved versions of iGluSnFR in its known green-fluorescing form, but it was further developed to emit blue, cyan and yellow fluorescence (**Marvin et al.**, **2018**). The tool became spectrally flexible while responding with faster kinetics, exerting higher glutamate sensitivity (200 μM), and showing greater SNR and photostability.

iGluSnFR reporter has been actively used to address important functional aspects of glutamatergic synapses. Among some findings, it revealed the extent of interaction between two major synaptic plasticity mechanisms, namely homeostatic and Hebbian plasticity (**Soares et al.**, **2017**), it gave insight into astrocytic glutamate clearance properties and modulation of its kinetics by synaptic activity (**Armbruster et al.**, **2016**), and it was reliably used for quantitative examination of the functional role of Synaptotagmin-1 in presynapse (**Vevea & Chapman**, **2020**). The probe was also used to examine mesoscale functional connectivity *in vivo* (**Xie et al.**, **2016**); however, by focusing on glutamate dynamics over a relatively wide region of interest. In this work, I have studied the potential of iGluSnFR for functional connectivity research with single-synaptic resolution *in vitro*.

2. RESEARCH OBJECTIVE

Neurons in neural networks display functional connectivity whereby they engage in various activity patterns while representing identical stimuli. This seeming stochasticity is governed by rules that are still largely unknown. Modulation of presynaptic activity is one mechanism that contributes to functional network formation. Thus, monitoring single synaptic activity is the key for understanding functional connectivity among neurons. Primary goal of this study is to assess the ability of a state-of-the-art optical reporter iGluSnFR to report subtleties in single synaptic activity in cultured networks, so that its potential for application in functional connectivity studies *in vitro* can be better understood. More specifically, I will:

1. Use iGluSnFR in a small-scale single-neuron model *in vitro* to characterize its baseline expression, sensitivity and source of fluorescence increase during synaptic activity,
2. Systematically address the ability of iGluSnFR to recapitulate well-defined presynaptic phenotype in genetically modified neurons,
3. Demonstrate the quantitative potential of iGluSnFR while uncovering differences in presynaptic activity of genetically modified and wild-type neurons.

3. MATERIALS AND METHODS

Throughout the study I have used neuronal cell cultures (WT, Tomosyn$^{-/-}$) generated by laboratory technicians or other scientists in the lab. I performed viral transfections of fluorescent probes on my own. I prepared imaging solutions and performed live iGluSnFR imaging. I conducted image and data analysis using own scripts and by designing own analysis pipelines. I chose and applied statistical tests on analyzed data. I designed and plotted all figures using own scripts. I wrote and designed algorithms for advanced peak detection.

3.1. Neuronal cultures

I used dissociated wild-type (WT) and Tomosyn floxed hippocampal neuron cultures which were prepared from E18.5 C57BL/6 mouse embryos (**Figure 3**), as first described in (**Mennerick et al., 1995**). Cerebral cortices were dissected in Hanks' balanced salt solution (Sigma, H9394) supplemented with 10 mM HEPES (Gibco, 15630-056). The hippocampi were isolated from the tissue and digested with 0.25% trypsin (Gibco, 15090-046) in Hanks' HEPES for 20 min at 37°C. Hippocampi were washed three times with Hanks' HEPES and triturated with fire-polished glass pipettes. Dissociated neurons were counted and plated in neurobasal medium (Gibco, 21103-049) supplemented with 2% B-27 (Gibco,17504-044), 1.8% HEPES, 0.25% Glutamax (Gibco, 35050-038), and 0.1% penicillin–streptomycin (Gibco, 15140-122). To prepare autaptic cultures, hippocampal neurons were plated in 12-well plates at a density of 1000-1500 cells/well on 18-mm glass coverslips containing micro-islands of rat glia. For glia preparations, newborn pups from female Wistar rats were used. Micro-islands were generated as previously described in (**Meijer et al., 2015**), by plating 8000/well rat glia on UV-sterilized agarose (Type II-A; Sigma, A9918)-coated etched glass coverslips stamped with a mixture of 0.1 mg/ml poly-D-lysine (Sigma, P6407), 0.7 mg/ml rat tail collagen (BD Biosciences, 354236), and 10 mM acetic acid (Sigma, 45731). At days *in vitro* (DIV) 1, Tomosyn floxed neurons were infected with Cre-recombinase to induce double Tomosyn knockout (Tomosyn$^{-/-}$). On DIV9, WT and Tomosyn$^{-/-}$ cultures were transduced with pFSynW-SFiGluSnFR.A184V and pSyn(pr)Synapsin-mCherry plasmids inserted in lentiviral backbone for iGluSnFR and synapsin-mCherry overexpression, respectively. Neurons were maintained in culture at 37°C and 5% CO2.

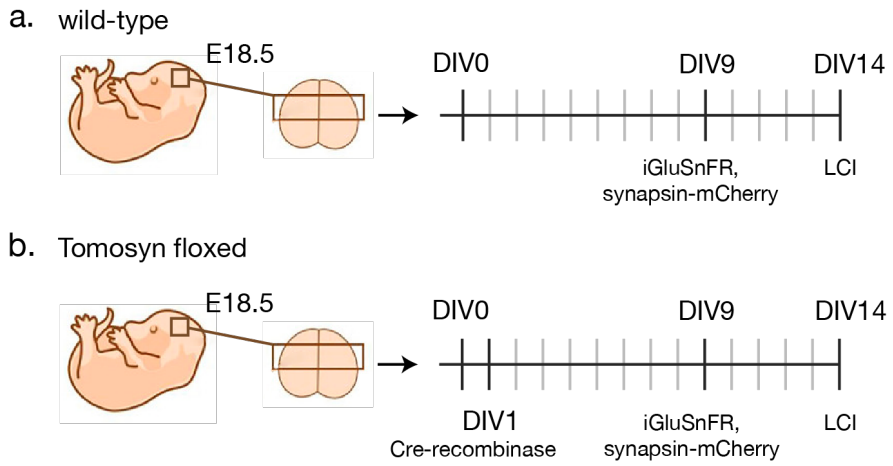

Figure 3. Timeline of culturing protocol. (a) Hippocampi from wild-type mouse pups were used to prepare primary neuronal culture. DIV, days *in vitro*. E, embryonic day. On DIV9, cultures were transfected with plasmids coding for fluorescent reporters. On DIV14, live-cell imaging (LCI) was performed. **(b)** Same as in (a.) but for Tomosyn$^{-/-}$ line generation. On DIV1, Tomosyn floxed cells were infected with Cre-recombinase. Embryo and brain illustrations taken from (**He et al.**, **2022**).

3.2. Live iGluSnFR imaging

Neurons were taken from culture at DIV14 and placed in an imaging chamber containing standard Tyrode solution (2 mM CaCl2, 2.5 mM KCl, 119 mM NaCl, 2 mM MgCl2, 30 mM glucose, 25 mM HEPES [pH 7.4]). Cultures were superfused with Tyrode throughout imaging. Imaging was performed under a widefield fluorescence microscope (Axiovert II, Zeiss; 40x objective, NA = 1.3) at room temperature controlled through MetaMorph 6 software (Molecular Devices). The illumination source was a mercury arc lamp (Zeiss). Images were acquired by an EM-CCD camera (Cascade). In each coverslip, 3-5 autaptic neurons were imaged. One still image of synapsin-mCherry fluorescence was taken per neuron for locating synaptic puncta. iGluSnFR fluorescence was recorded in stream acquisition mode at 10 Hz acquisition rate (100 ms exposure time, 2x binned). Electrical stimulation was applied using a local-field potential (LFP) electrode (WPI), with stimulation intensity 30 mV/pulse. Stimulation protocols were written in Master 8 software (AMPI).

In Figure 6a,b, a neuron was imaged in Tyrode for 1 min after which 1 µM tetrodotoxin (TTX; Sigma) was acutely applied to the same culture (2 min incubation). For Figure 6c,d, neurons were incubated in 1 µM TTX for 2 hours prior to imaging.

3.3. Image analysis

Recordings were analyzed in Fiji/Imagej (National Institutes of Health) using custom-written script (template kindly provided by Moro A.). First, top-hat transform was applied to a still image of a neuron expressing synapsin-mCherry to extract highly saturated, small 3-by-3 pixel elements corresponding to synaptic puncta. Individual synaptic coordinates, or regions of interest (ROIs), were then transferred to time-lapse recording containing iGluSnFR fluorescence. Gray pixels in the 3-by-3 region were averaged per ROI/synapse in every frame. Average gray pixel values reflecting iGluSnFR fluorescence over time from all ROIs were saved per neuron. When neurons were imaged over multiple stimulation protocols (baseline + 5 APs at 0.75 Hz, 5 APs at 2 Hz and 100 APs at 40 Hz + 2 recovery pulses), synaptic traces from separate recordings were concatenated into a continuous trace for convenience. In case of field-of-view (FOV) shift between recordings, FOV correction was manually performed for precise synaptic positioning.

3.4. Data analysis

3.4.1. Raw trace normalization

Raw synaptic traces per neuron were analyzed and visualized in Matlab (MathWorks) using custom-written scripts and analysis pipelines. Baseline fluorescence (F_0) was calculated per synaptic trace from the initial part of recording as an average of gray pixel values over 10 frames (1 s). Individual fluorescence traces were normalized to their baseline as: F/F_0. Traces from imaging sessions longer than 20 s were detrended using moving median approach with arbitrary window size chosen based on *a priori* exploration. Window sizes were consistent throughout the experiment but were specific per recording (9.9 s for traces containing 0.75 Hz stimulation; 10.1 s for traces with 2 Hz stimulation; 40 Hz traces were not detrended).

3.4.2. Quantification of synaptic responses

Peak responses to stimulation were calculated as change in fluorescence intensity over baseline as: $\Delta F/F_0 = (F_t - F_0)/ F_0$, where F_t is fluorescence intensity at stimulation time *t*. In figures showing average iGluSnFR fluorescence over all synapses (e.g, Figure 6c, Figure 7b,d),

mean ± STD $\Delta F/F_0$ were quantified from 1 frame with time *t* in which synapses were theoretically expected to respond based on stimulation settings. Due to occasional instances of delayed communication between stimulation-triggering software and equipment, some stimulation pulses were delivered 0.1 s later and were misaligned with expected frames (1 frame delay). Also, in some synapses there was a natural 0.1 s delay in peak response to stimulation. So, for calculating average synaptic responses per neuron (e.g., Figure 7c,e), a custom-written algorithm was used to precisely detect delayed peaks around stimulation frames. The algorithm searched for maximal $\Delta F/F_0$ in *t-1*, *t* and *t+1* for every pulse during 0.75 Hz stimulation, and in *t* and *t+1* for pulses during 2 Hz stimulation. That way, synaptic responses that peaked with 1-frame delay were included with their real amplitude for increased robustness during statistical comparison.

In Figure 7e, kinetics of iGluSnFR were too slow to capture shapes of individual APs during 40 Hz stimulation. This resulted in a step-like signal with duration of 2.5 s which is exactly the time needed to deliver 100 AP. With frame duration of 100 ms and inter-spike interval of 25 ms, there are 100/25 = 4 APs per stimulation frame. Therefore, $\Delta F/F_0$ from the 1st frame was divided with 4 to get the 1st-evoked $\Delta F/F_0$ response during 40 Hz stimulation.

3.4.3. mGT detection

Custom-designed pipeline was used to detect mGT events from individual synaptic traces. First, 7 random cells (3 WT, 4 Tomosyn$^{-/-}$) were chosen from 1 culturing week and an advanced peak-detection algorithm (thresholding algorithm, (**van Brakel**, **2020**)) was used to detect peaks in the baseline signal (59.8 s) from all synaptic traces. Fluorescence values crossing the threshold of 4 STDs away from moving mean (moving window size = 10.1 s) were detected as mGTs. Then, detected mGTs from analyzed synapses were manually classified in a custom-written GUI to confirm true positives (TPs) and true negatives (TNs), add false negatives (FNs) and remove false positives (FPs). Additional analysis on inhibitory neurons was used to understand properties of FPs. Five inhibitory neurons were imaged and stimulated, synapses were detected and traces were normalized and detrended as described above. Peaks in inhibitory synaptic traces were detected using the same settings in the thresholding algorithm used for excitatory cells prior to manual classification. All detected peaks represent TNs because inhibitory neurons do not release glutamate. Manual peak classification was used to obtain reference values for $\Delta F/F_0$ amplitude and SNR (**Figure 4**). These two parameters, along

with signal gradient, signal shape and signal decay, were then used for automated scoring of peaks during bulk detection of mGTs over all neurons.

Bulk mGT detection in baseline synaptic signal from all neurons was performed using built-in Matlab function *findpeaks* with low threshold for peak amplitude ($\Delta F/F_0 = 0.09$) and minimal distance of 1s between consecutively detected peaks. This resulted in many FP peaks; however, they were rigorously evaluated using the scoring approach described above. Peaks which scored well (> 10 points, arbitrary value) were accepted as mGT events. This approach was applied uniformly for WT and Tomosyn$^{-/-}$ synapses.

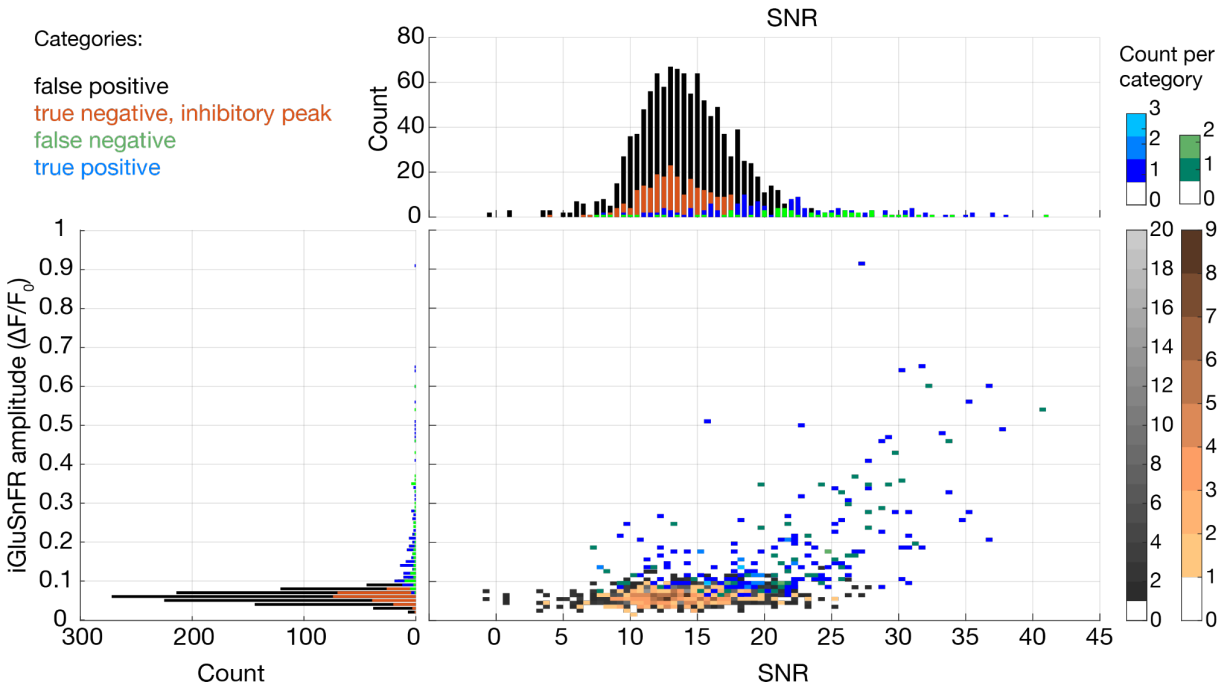

Figure 4. Outcome of manual peak classification. Distributions of signal-to-noise (SNR) ratios (top) and $\Delta F/F_0$ amplitudes (left) of classified peaks. Merging of the two distributions (heatmap). Color codes match across the heatmap and distributions. SNR distribution shares the x axis with heatmap. Amplitude distribution shares the y axis with heatmap.

3.4.4. Synaptic participation

Synaptic participation to 0.75 Hz stimulation was obtained by evaluating synaptic responses in windows centered around precise timings of 5 APs (window size = 1.3 s). Full 1.3 s signal was analyzed per synapse using the scoring method developed for mGT evaluation described above, but with modified settings to detect AP-like signal. Above threshold activity

was registered per synapse for 5 APs in a binary matrix containing active and non-active synapses, as in Figure 9a (left). Binary matrix was obtained per neuron, and was summed over all synapses across 5 columns representing 5 APs to get the number of participating synapses, as in Figure 9a (center). Participation count per AP was divided with total number of synapses to get the percentage of synaptic participation during 0.75 Hz, as in Figure 9a (right). The approach was identical for 2 Hz stimulation, but only the 1st-evoked responses were evaluated (window size = 0.7 s) due to insufficient amount of data points across 2nd-to-5th-evoked to account for reliable analysis.

3.4.5. Presynaptic pool dynamics

The initial exocytosis rate triggered by 40 Hz stimulation was obtained from slope of instantaneous decay after fitting 2nd-order exponential decay function to individual synaptic responses to 100 APs. Decay function was described as $y(x) = Ae^{mx_1} + Be^{nx_2}$, where x_1 was instantaneous slope, x_2 was secondary slope, and A, B, m and n were constants (A and B were unique for every synapse; m = -0.7; n = -0.25). Negative inverse of the instantaneous slope ($-1/x_1$) represents the time constant of the initial exocytosis rate. Secondary slope represents the rate of exo-/endocytosis, and its time constant was calculated as $-1/x_2$. Probe decay time constant was calculated by fitting 1st-order exponential decay function ($y(x) = Ae^{-mx}$) to synaptic traces immediately after 40 Hz stimulation, and then obtaining negative inverse of its slope ($-1/x$).

To quantify recovery, peak prominence was calculated for the 1st frame during the 100 AP train at 40 Hz, and for 1st and 2nd recovery pulses by calculating distance between F_0 and peak $\Delta F/F_0$ amplitude in corresponding frames. Ratio between prominence of 1st-evoked (p_{e1}) and 1st recovery pulse (p_{r1}) was calculated per synapse as: p_{r1}/p_{e1}, to monitor synaptic recovery 1 s after 40 Hz train. Likewise, prominence ratios were calculated for 1st-evoked and 2nd recovery pulse (p_{r2}/p_{e1}, where p_{r2} is 2nd pulse prominence) to monitor synaptic recovery 4 s after.

3.5. Statistical analysis

Statistical analysis was performed in Matlab (MathWorks). Data were reported using standard descriptive statistical parameters: mean ± standard deviation (STD), and median

values. In boxplots, interquartile range between 25th and 75th percentile, with median, minimal and maximal values were reported. Percentage difference in synaptic responses between compared $\Delta F/F_0$ was calculated as: $(x_2 - x_1)/x_1$, where x_1 is previous $\Delta F/F_0$ value and x_2 is new $\Delta F/F_0$. Coefficient of variation (CoV) in Figure 5 was calculated as STD/mean.

Data were presumed to be non-normally distributed so nonparametric Wilcoxon rank-sum and Mood's median tests were used for comparison of independent samples throughout the study. Significance was reported as: n.s., not significant; * $p < 0.05$; ** $p < 0.01$; *** $p < 0.005$; **** $p < 0.001$. In case of multiple comparisons, Bonferroni correction of p value was applied.

4. RESULTS

4.1. General evaluation of the iGluSnFR probe

4.1.1. iGluSnFR reporter shows reliable expression in autaptic neuronal cultures

To address the ability of iGluSnFR for presynaptic activity quantification in the network, I used a smaller-scale experimental model of single neurons in autaptic cultures (**Figure 5a**). Autaptic neuronal cultures are unique in that the neuron forms self-synapses (autapses) which are functionally identical to (hetero) synapses and can be reliably used to study synaptic properties (**Meijer et al., 2019**). Wild-type neurons in autaptic cultures expressed synapsin-mCherry to locate synaptic puncta and iGluSnFR to monitor synaptic activity (**Figure 5b**). I evaluated general characteristics of iGluSnFR expression in autapses to get a better understanding of the probe's behavior *in vitro*. The average number of clearly detectable synapses per neuron was 211.05 ± 126.26 (55 neurons, 3 culturing weeks; **Figure 5c**). This gives access to more than 10 000 synapses per experiment. Average of raw iGluSnFR fluorescence across synapses was similar in neurons across different cultures (**Figure 5d**). I quantified coefficients of variation (CoV) in baseline fluorescence (F_0) from all synapses per neuron to compare variability between synapses. I detected maximal and minimal CoV in synaptic F_0 values of 0.69 and 0.16, respectively (**Figure 5e**). Average between-synapse CoV from all recorded neurons was 0.40 ± 0.14 (55 neurons).

4.1.2. Neuronal glutamate release and spontaneous synaptic vesicle fusion underlie increase in iGluSnFR intensity

Next I aimed at understanding the source of iGluSnFR fluorescence intensity increase in autaptic cultures. It is crucial to validate whether iGluSnFR signal comes from AP-mediated glutamate release or from other potential sources like astrocytes (**Harada et al., 2016**). To test that, I first imaged cultured excitatory neurons in 2 mM Ca^{2+} solution representing a naive condition (**Figure 6a**). I applied 10 AP-evoking electrical impulses at 2 Hz, which is frequency slow enough for the iGluSnFR probe to resolve rise and decay times of single APs (**Marvin et al., 2013**). I repeated the same imaging protocol with cultured neurons incubated in 1 μM of tetrodotoxin (TTX; **Figure 6a**). TTX blocks propagation of AP along the axon by blocking Na^+ channels, thus resulting in no SV release from presynapse upon electrical stimulation of the

neuron. Indeed, the naive condition resulted in $\Delta F/F_0$ peaks precisely aligned with stimulation times which are absent in TTX condition (**Figure 6b**). I detected $\Delta F/F_0$ increase of about 0.14 ± 0.17 for the first evoked AP in naive condition, and noise level fluctuations in $\Delta F/F_0$ for TTX treated condition (**Figure 6c**). These results validated the use of iGluSnFR probe to report AP-triggered release of neuronal glutamate. Remarkably, the probe reported spontaneous SV fusion events during baseline recording from single synapses. These events are miniature glutamate transients (mGTs), and were detected in both naive and TTX conditions since they are independent of AP (**Figure 6d**).

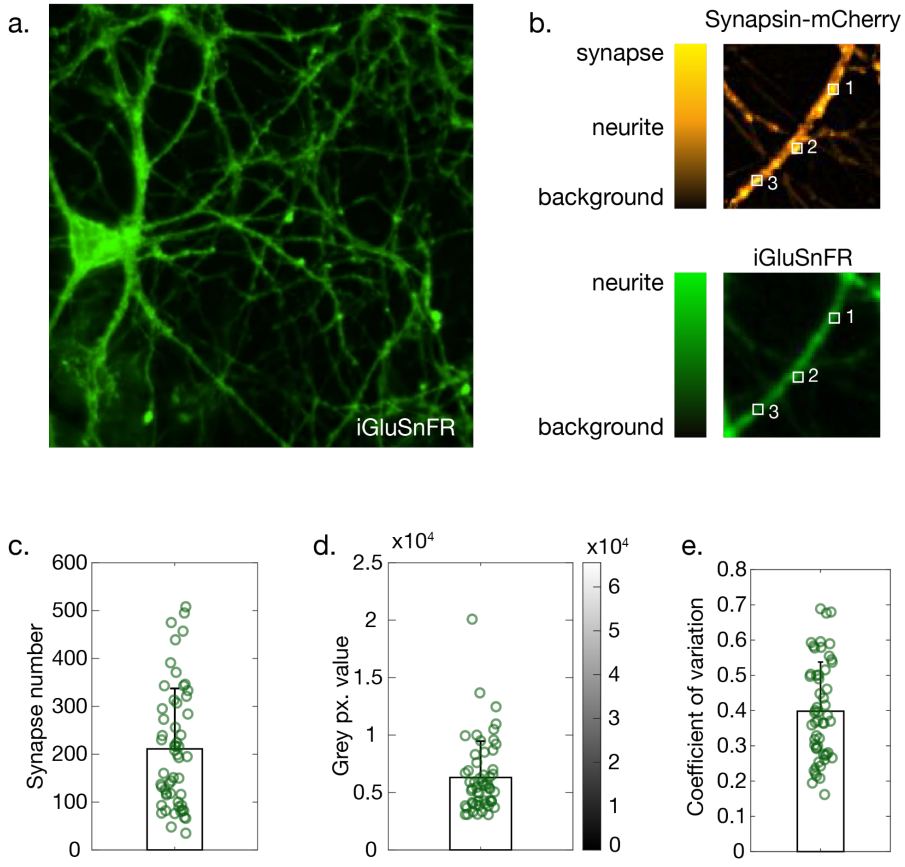

Figure 5. Overview of iGluSnFR expression in autaptic neuronal cultures. (a) An example neuron expressing iGluSnFR in culture. **(b)** Synapsin-mCherry mask used to detect synaptic puncta (top). Synaptic coordinates were transferred to iGluSnFR mask to extract activity (bottom). White squares, three example synaptic coordinates. **(c)** Average number of synapses per neuron (n = 55, 3 independent weeks). **(d)** Average baseline iGluSnFR fluorescence (F_0) per neuron (n = 55). Colorbar, 16-bit grayscale pixel gradient. Black, background; gray, signal. **(e.)** Coefficient of variation between synaptic F_0 values per neuron (n = 55).

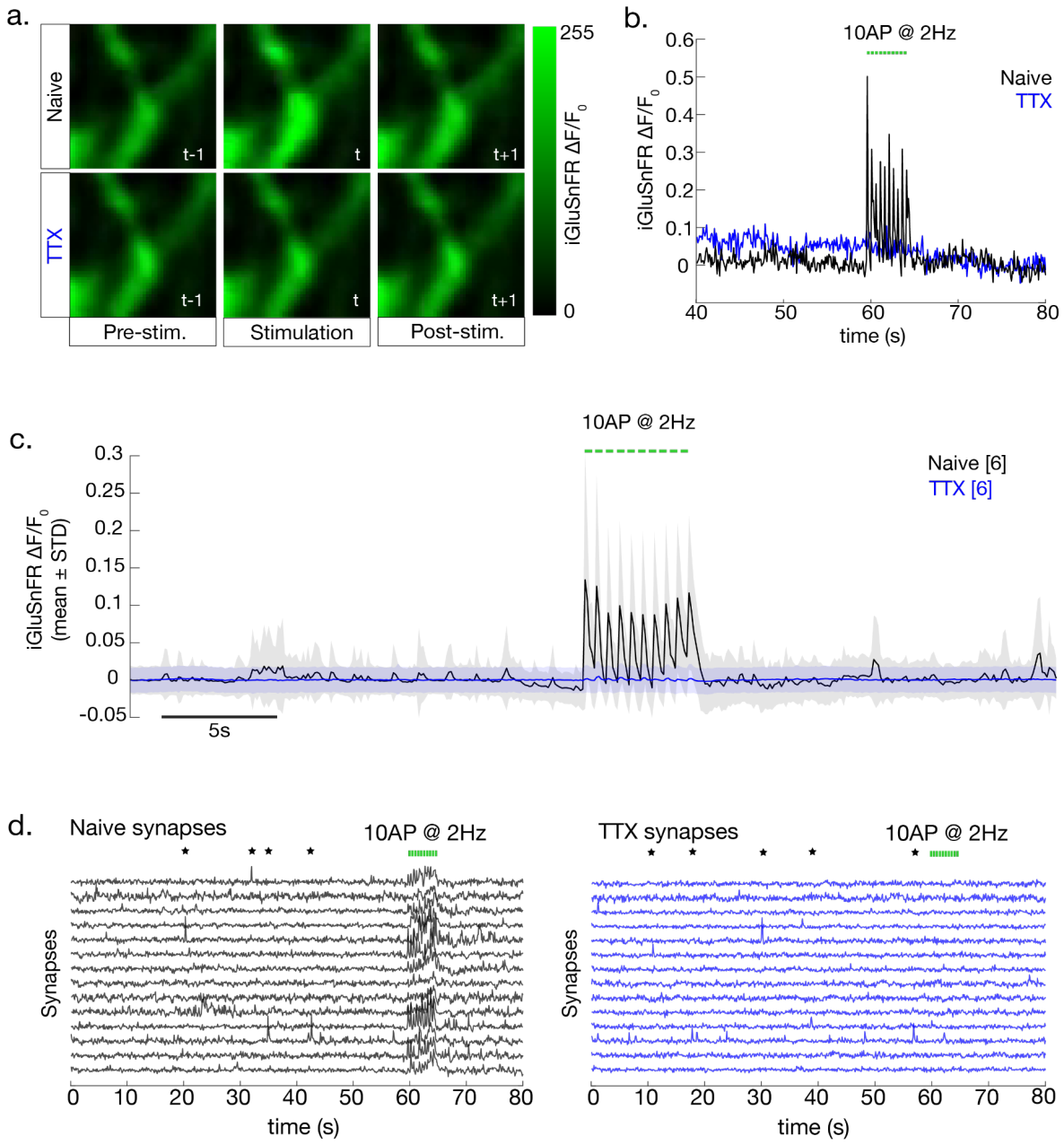

Figure 6. Change in iGluSnFR fluorescence upon neuronal glutamate release. **(a)** Single synapse in naive (top row) and TTX conditions (bottom row) one frame before (t-1) and after (t+1) the first stimulation pulse at time t. **(b)** Synaptic responses to 10 APs at 2 Hz form synapses in (a). Black, naive. Blue, TTX. **(c)** Average activity before, during and post stimulation with 10 AP at 2 Hz in naive (black) and TTX (blue) conditions (6 neurons). **(d)** Evoked (below green lines, simulation times) and spontaneous (*) synaptic activity from naive (left) and TTX-treated (right) synapses (n = 14).

4.2. Advanced iGluSnFR evaluation in genetically modified presynapse

4.2.1. iGluSnFR recapitulates the well-known phenotype in Tomosyn$^{-/-}$ neurons

iGluFnSR activity reliably reflects presynaptic glutamate release. The probe was previously used to report strong presynaptic phenotypes like the loss of synchronous SV release when presynaptic release machinery is disrupted (**Vevea & Chapman**, **2020**). Functionally altered synapses may exert only subtle differences in their activity. Here, I studied whether iGluSnFR can reflect these subtleties in model neurons absent from the presynaptic protein Tomosyn (Tomosyn$^{-/-}$ neurons). They respond with increased amplitude of first-evoked neuronal response and show increased frequency of spontaneous events when compared to WT (**McEwen et al.**, **2006**; **Sauvola et al.**, **2021**).

I first looked into whether the iGluSnFR probe reports 1st-evoked response phenotype. I stimulated neurons with 5 AP-evoking pulses at 0.75 and 2 Hz frequency. First, 0.75 Hz stimulation evoked synaptic responses with precisely aligned iGluSnFR peaks to expected AP-timings (**Figure 7a**). First-evoked responses show differences in $\Delta F/F_0$ amplitudes between genotypes, while consecutive responses (2nd-to-5th) have comparable $\Delta F/F_0$. Since this might be the case for few rather than all Tomosyn$^{-/-}$ synapses, I averaged synaptic response from 39 WT and 49 Tomosyn$^{-/-}$ neurons to get clearer insight in overall synaptic activity per group (8712 and 10891 synapses, respectively; 3 imaging weeks). Averaged responses revealed that Tomosyn$^{-/-}$ synapses peak with 0.17 ± 0.23 $\Delta F/F_0$ (mean ± STD) during 1st-evoked activity, and respond with about 53% lower $\Delta F/F_0$ amplitude immediately after (2nd AP: 0.08 ± 0.14 $\Delta F/F_0$). The following Tomosyn$^{-/-}$ responses showed sustained amplitudes similar to 2nd-evoked (3rd AP: 0.08 ± 0.15 $\Delta F/F_0$; 4th AP: 0.05 ± 0.11 $\Delta F/F_0$; 5th AP: 0.06 ± 0.12 $\Delta F/F_0$; **Figure 7b**, blue). Furthermore, average responses in WT synapses revealed a dramatic difference in 1st AP amplitude from Tomosyn$^{-/-}$ synapses. WT synapses respond with 0.06 ± 0.13 $\Delta F/F_0$ on average, unlike 183% stronger response seen in Tomosyn$^{-/-}$ (**Figure 7b**, black). Unlike in Tomosyn$^{-/-}$ synapses, 1st-evoked response in WT showed very little difference from 2nd AP, during which synapses respond with 0.06 ± 0.09 $\Delta F/F_0$ on average. These were higher than amplitudes of consecutive APs (3rd AP: 0.03 ± 0.05 $\Delta F/F_0$; 4th AP: 0.03 ± 0.07 $\Delta F/F_0$; 5th AP: 0.02 ± 0.04 $\Delta F/F_0$).

Evoked peak synaptic responses were averaged per neuron. I tested differences in 1st-evoked response amplitudes between genetically altered synapses, as well as genetically identical synapses (**Figure 7c**). Among evoked responses in the WT group, a statistically significant decrease in response was detected only between 1st and 5th AP. In the Tomosyn$^{-/-}$ group, 3rd, 4th and 5th APs show significantly lower response when compared with 1st. In addition, significance was found in iGluSnFR-based increase of 155% in 1st-evoked response in Tomosyn$^{-/-}$ synapses *versus* WT (0.23 ± 0.12 $\Delta F/F_0$, 0.09 ± 0.10 $\Delta F/F_0$, respectively). (For discrepancies in mean ± STD $\Delta F/F_0$ values reported from average of all synapses *versus* average from all neurons, see Materials and Methods.) Interestingly, when I compared $\Delta F/F_0$ peaks from other APs between WT and Tomosyn$^{-/-}$ groups (i.e., 2nd-evoked WT to 2nd-evoked Tomosyn$^{-/-}$ etc.), none showed significant difference (data not shown; $p > 0.05$ for all, Wilcoxon rank-sum, after Bonferroni correction).

I further looked into synaptic responses to a faster, 5 APs at 2 Hz stimulation. I averaged over individual synaptic traces from all neurons per group (**Figure 7d**). Similarly to prior results, Tomosyn$^{-/-}$ synapses respond with 0.16 ± 0.19 $\Delta F/F_0$ on average during 1st-evoked AP. That was a 78% stronger response than average across all WT synapses where I detected $\Delta F/F_0$ = 0.09 ± 0.12. I then averaged peak responses per neuron (**Figure 7e**). In WT neurons, 4th and 5th APs significantly decrease in response strength from the 1st response. Moreover, average synaptic responses to all but 2nd AP in Tomosyn$^{-/-}$ neurons have significantly decreased peak amplitudes when compared to 1st-evoked AP (**Figure 7e**, right). A major observation from 0.75 Hz stimulation responses was detected here as well. Tomosyn$^{-/-}$ neurons consistently respond with stronger amplitude to 1st-evoked stimulation (0.19 ± 0.20 $\Delta F/F_0$), which is a significant 90% increase when compared to WT responses (0.10 ± 0.12 $\Delta F/F_0$). Lastly, I analyzed 1st-evoked synaptic responses to very fast stimulation during which synapses were challenged with 100 APs at 40 Hz to test extreme activity mode (**Figure 7e**). Tomosyn$^{-/-}$ synapses on average show 100% increased peak $\Delta F/F_0$ compared to WT response (see Materials and Methods for 1st-evoked response approximation). This difference proved significant when responses were averaged per genotype ($p < 0.01$, Wilcoxon rank-sum), and was not tested when averaged per neuron.

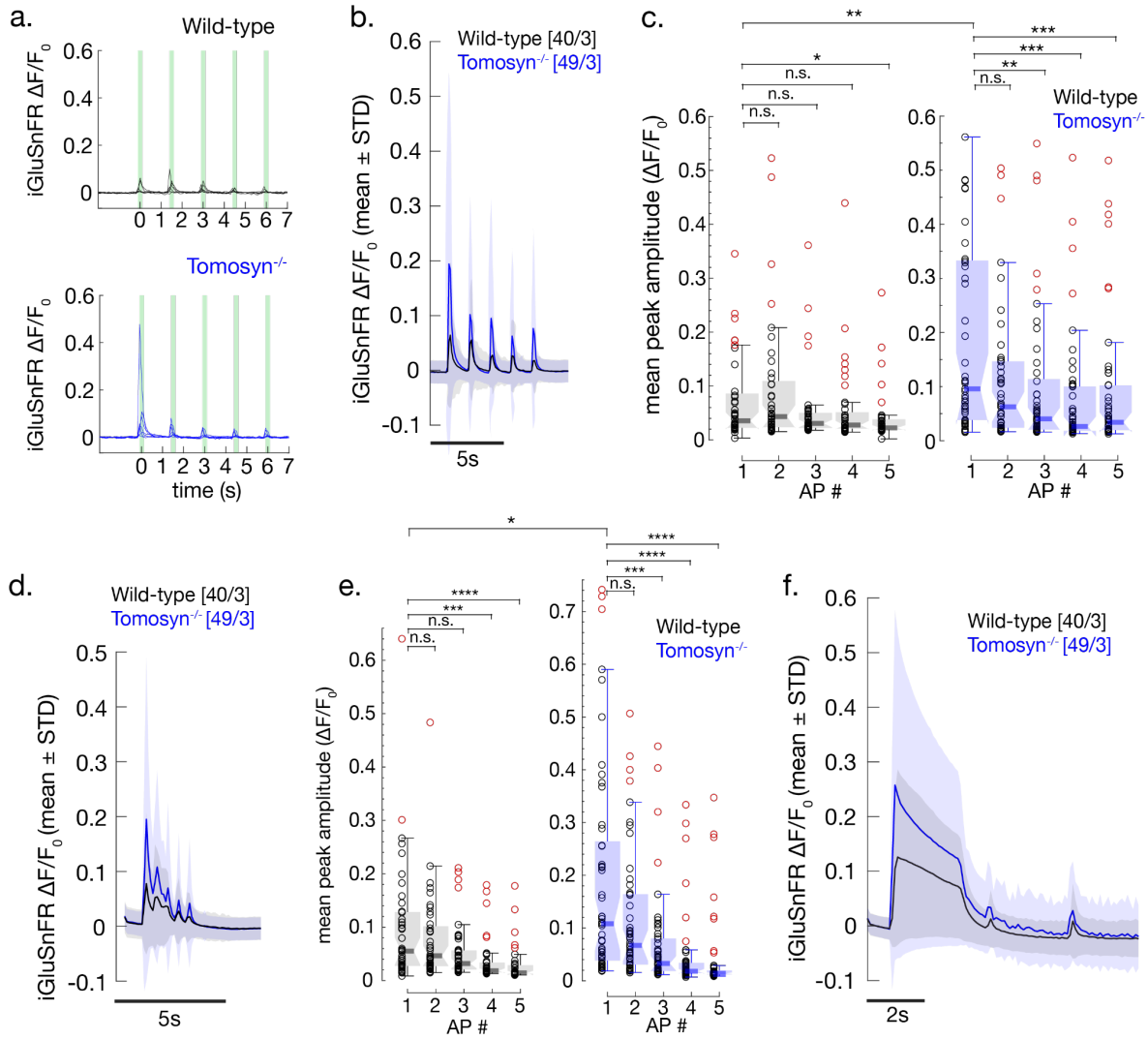

Figure 7. Differences in synaptic response between Tomosyn$^{-/-}$ and Wild-type (WT) neurons reported by iGluSnFR. (a) Evoked responses from WT (n = 6; top) and Tomosyn$^{-/-}$ (n = 7; bottom) synapses to 5 APs at 0.75 Hz.Time in seconds is aligned to the onset of the first pulse. **(b)** Average from evoked synaptic responses to 5 AP at 0.75 Hz. Solid trace, mean; shade, STD. Black, WT (39 neurons); blue, Tomosyn$^{-/-}$ (49 neurons). **(c)** Average peak response per AP pulse from responses in (b). Red circles, outliers. Black boxplots, WT; blue boxplots, Tomosyn$^{-/-}$ neurons. Boxplots show interquartile range between 25th and 75th percentile (lower and upper box boundary, respectively), with median (solid horizontal line). Whiskers show minimal (lower thin horizontal line) and maximal (upper thin horizontal line) values. Significance tested with Wilcoxon rank-sum test, Bonferroni correction (n.s., not significant; * $p < 0.05$; ** $p < 0.01$; *** $p < 0.005$; **** $p < 0.001$). Note that due to visualization purposes, y axes were concatenated which made some outliers not appear on the figure. **(d)** Same as in (b) but for 5 AP at 2 Hz stimulation type. **(e)** Same as in (c) but for 5 AP at 2 Hz stimulation type. **(f)** Same as in (b) but for stimulation type containing 100 AP at 40 Hz followed by two recovery pulses.

4.2.2. Subthreshold detection using iGluSnFR confirms increased spontaneous activity in Tomosyn$^{-/-}$ synapses

Another hallmark of Tomosyn$^{-/-}$ phenotype describes increased spontaneous activity below AP threshold. I have demonstrated earlier that iGluSnFR has capacity for subthreshold mGT event detection (see Chapter 4.1.2.), although just qualitatively. Here I quantitatively address the ability of iGluSnFR to report increased frequency of subthreshold events in Tomosyn$^{-/-}$ neurons. WT and Tomosyn$^{-/-}$ neurons were imaged for 60 s prior to evoking responses with 0.75 Hz stimulation. During the pre-stimulation period i.e., baseline, it is likely that SVs from individual synapses spontaneously fuse with the presynaptic membrane, causing glutamate release. I developed an advanced peak-detection algorithm to detect mGT events in baseline (**Figure 8a**; see Materials and Methods) It captured 200 spontaneous events in WT synapses and 1739 events in Tomosyn$^{-/-}$ synapses (8712 WT and 10891 Tomosyn synapses analyzed; 39 and 49 neurons, respectively). When averaged over all detected events per genotype, their shape showed remarkable similarity (**Figure 8b**). To see if peak mGT amplitudes significantly differ, I extracted peak $\Delta F/F_0$ from all mGT events and looked at their distribution per genotype (**Figure 8c**). Due to skewness in both distributions, I statistically compared group $\Delta F/F_0$ medians (**Figure 8c**, vertical lines). Interestingly, they do not show a significant difference between genotypes (WT median $\Delta F/F_0 = 0.13$, Tomosyn$^{-/-}$ median $\Delta F/F_0 = 0.14$; $p = 0.1374$, Mood's median test).

In addition, I compared subthreshold event frequency between groups (**Figure 8d**, left). Average synaptic mGT frequency was 0.81 ± 1.62 Hz in Tomosyn$^{-/-}$ neurons, and 0.13 ± 0.29 Hz in WT neurons. This marked more than 500% increase in frequency and was significant. Lastly, I have shown that on average, Tomosyn$^{-/-}$ neurons have about 350% higher fraction of synapses that undergo spontaneous SV fusion leading to mGT events than WT neurons. In WT neurons, that was only 3.81 ± 0.18% of synapses while in Tomosyn$^{-/-}$ neurons there were 17.46 ± 28.44% synapses showing mGTs. Moreover, these differences were statistically significant (**Figure 8d**, right).

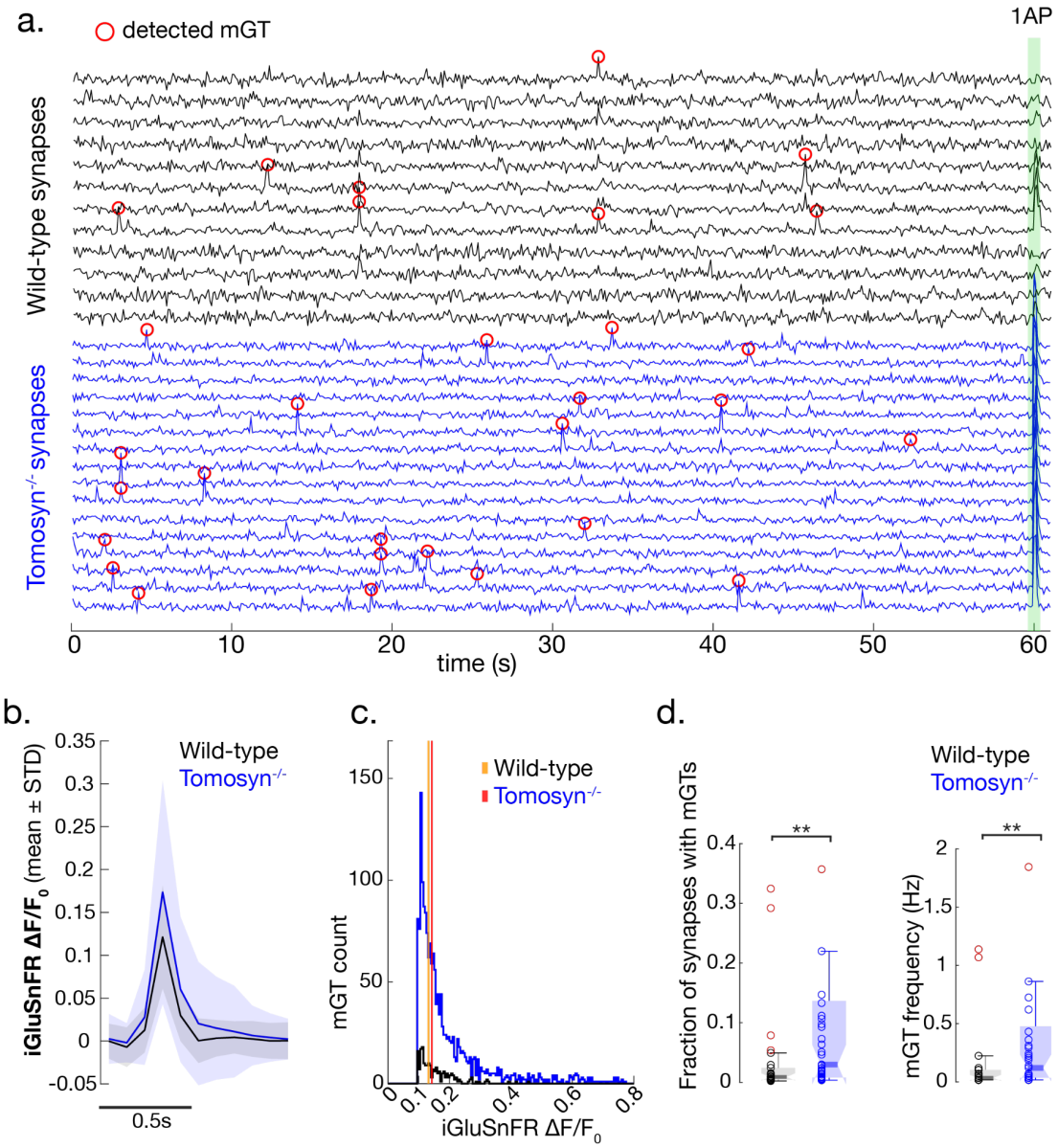

Figure 8. Detection of spontaneous synaptic events below threshold. **(a)** Spontaneous synaptic events (mGTs) in baseline. Red circles, detected events. Black traces, individual WT synapses (n = 12). Blue traces, Tomosyn$^{-/-}$ synapses (n = 16). Green bar, evoked activity to 1 AP. **(b)** Average shapes of WT (black, n = 200) and Tomosyn$^{-/-}$ (blue, n = 1739) mGT events. Solid line is mean; shade is STD. **(c)** Distributions of detected mGT amplitudes per genotype. Vertical bars, distribution medians (orange, WT; red, Tomosyn$^{-/-}$). Note that Tomosyn$^{-/-}$ mGT amplitudes go up to 1.4 but were left out for visualization purposes. **(d)** Fraction of synapses showing spontaneous activity per genotype (left), and genotype-specific frequency of spontaneous events per synapse (right). Circles, average per neuron; red, outliers. Boxplot description and statistical analysis same as in Figure 6c.

4.3. iGluSnFR imaging reveals detailed functional properties of Tomosyn$^{-/-}$ synapses

4.3.1. Synaptic participation is higher in Tomosyn$^{-/-}$ synapses

Biological explanation for increased 1st-evoked response in Tomosyn$^{-/-}$ neurons is still an open question (**Ashery et al., 2009**). With iGluSnFR, an answer might be a step closer since it allows resolving single synapse-related hypotheses. One of the plausible explanations for increased neuronal activity in absence of Tomosyn is higher synaptic participation in overall neuronal response. I examined synaptic participation per evoked response in Tomosyn$^{-/-}$ *versus* WT neurons to the previously introduced 0.75 (**Figure 9a**) and 2 Hz stimulation patterns (**Figure 9b**). In case of 0.75 Hz stimulation, average synaptic participation in WT neurons for 1st-evoked AP was 22.66 ± 29.12% (group median 10.54%; **Figure 9c**, top). A total of 31 neurons showed active participation, with about 73 contributing synapses per neuron (total of 2276 detected active WT synapses). Tomosyn$^{-/-}$ synapses participated with 97% increased rates which were 44.74 ± 36.13% on average per neuron (group median 41.61%; **Figure 9c**, bottom). I found 45 neurons with active 1st-evoked responses, having approximately 115 contributing synapses (a total of 5177 active Tomosyn$^{-/-}$ synapses were detected). Difference in participation to 1st-evoked AP between genotypes was highly statistically significant ($p < 0.01$, Wilcoxon rank-sum, after Bonferroni correction). Participation was decreased for all other APs for Tomosyn$^{-/-}$ synapses (medians for 2-5 APs: 17.14%, 9.76%, 2.75% and 4.33%, respectively), and remained similar or decreased for WT synapses (medians for 2-5 APs: 11.82%, 2.36%, 3.49% and 0.99%, respectively).

Similar results were obtained from responses to 2 Hz stimulation. I found 36 WT and 48 Tomosyn$^{-/-}$ neurons which showed 1st-evoked participation. There were around 67 and 95 synapses per neuron, respectively, actively responding to 1st-evoked activity (total of 2419 for WT and 4573 for Tomosyn$^{-/-}$). The average WT neuron had a synaptic participation rate of 27.33 ± 29.79% (group median 12.20%; **Figure 9d**, top). In absence of Tomosyn, synapses showed 40% higher participation to the first 2 Hz pulse which was 38.18 ± 25.18% on average (group median 30.36%; **Figure 9d**, bottom). Although change in participation between genotypes is apparent, it was not statistically significant ($p = 0.0796$, Wilcoxon rank-sum; $p > 0.05$, Mood's median test).

Moreover, because I previously observed significant differences between AP amplitudes from synapses with the same genotype (**Figure 7c**), I quantified synaptic participation during 2nd-to-5th AP at 0.75 Hz for WT and Tomosyn$^{-/-}$ neurons to see if it explains the effect. I compared synaptic participation results the same way it was compared for peak $\Delta F/F_0$ responses i.e., between 1st- and subsequently-evoked APs within the same group. Interestingly, trends of average $\Delta F/F_0$ response peaks and average synaptic participations match in both WT and Tomosyn$^{-/-}$ groups (trends were estimated from relative median positions in **Figure 7c** and **Figure 9c** per AP). As shown previously, differences between 1st- and other-evoked $\Delta F/F_0$ amplitudes in WT were non-significant for all but 5th AP. Here, synaptic participation in WT likewise showed non-significant difference for 2nd, 3rd and 4th AP, but proved non-significant for 5th AP difference (**Figure 9c**, top). However, I found a strong pairwise correlation between average 5th-AP participation rates and amplitudes per neuron (correlation coefficient of 0.97). In case of Tomosyn$^{-/-}$ neurons, statistical differences in evoked iGluSnFR amplitudes matched statistical results in synaptic participation data (**Figure 9c**, bottom). These results suggest that synaptic participation likely underlies differences in evoked $\Delta F/F_0$ amplitudes from 2 Hz synaptic responses as well, from which it was hard to reliably extract participation rates for 2nd-to-5th AP, so significance in participation differences was not tested beyond 1st-evoked AP.

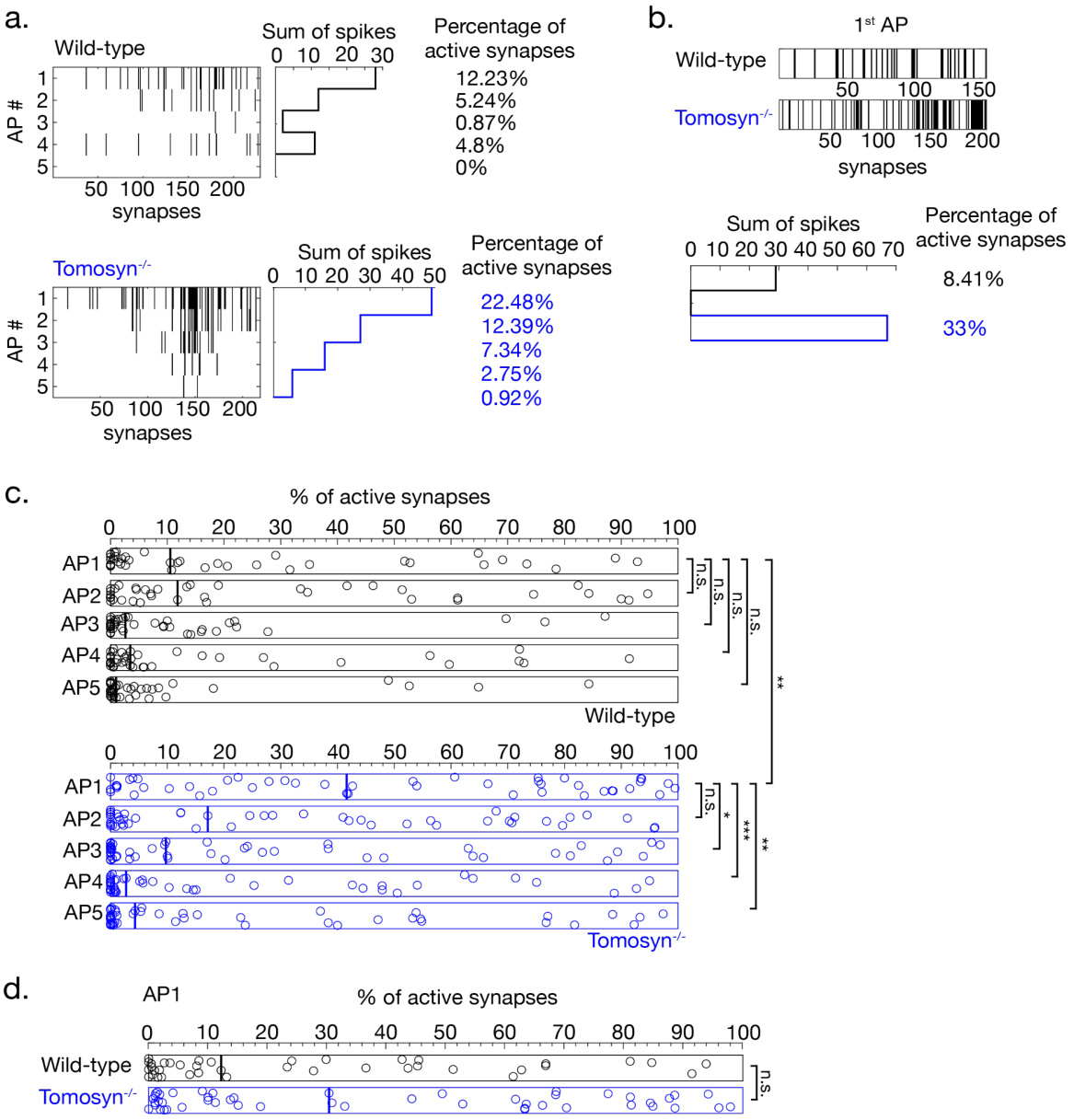

Figure 9. Quantification of synaptic participation during evoked activity. **(a)** Raster plot of synaptic activity per 5 APs during 0.75 Hz stimulation for 1 WT (top left) and 1 Tomosyn$^{-/-}$ neuron (bottom left). Rows, 5 APs; columns synapses. Black lines, active synapse. White space, non-active synapses. Number of active synapses can be summed per AP (top middle, WT; bottom middle Tomosyn$^{-/-}$). Percentage of active synapses per AP (top right, WT; bottom right, Tomosyn$^{-/-}$). **(b)** Same as in (a) but for 2 Hz stimulation and activity of first-evoked AP only (bottom). **(c)** Average synaptic participation to 5APs at 0.75 Hz per neuron (39 WT, black; 49 Tomosyn$^{-/-}$, blue). Solid vertical line, median. **(d)** Same as in (c) but for 1st-evoked in 2 Hz stimulation. Significance was tested with Wilcoxon rank-sum test, with Bonferroni correction (n.s., not significant; * $p < 0.05$; ** $p < 0.01$; *** $p < 0.005$; **** $p < 0.001$).

4.3.2. Tomosyn$^{-/-}$ synapses potentially fuse multiple SVs

Synaptic participation differs between Tomosyn$^{-/-}$ and WT neurons; however, I asked whether it fully accounts for the observed increase in 1st-evoked amplitude in absence of Tomosyn. Because of Tomosyn's putative role in SV docking, a plausible additional mechanism might involve an increased number of SVs fusing per Tomosyn$^{-/-}$ synapse. To test that, I considered only the active synapses and their peak $\Delta F/F_0$ amplitude during 1st-evoked APs from 0.75 Hz and 2 Hz stimulations. I have also taken advantage of mGT amplitudes. Since mGTs are known to be single-SV fusion events, comparing amplitudes of spontaneous and evoked $\Delta F/F_0$ should give a strong intuition for approximating the number of released vesicles.

I detected active synaptic participation in 31 WT and 45 Tomosyn$^{-/-}$ neurons during 1st AP at 0.75 Hz stimulation. When average shapes of 1st-evoked responses are compared between active synapses only, there is 86% amplitude increase in the Tomosyn$^{-/-}$ group with respect to WT (**Figure 10a**, left). Tomosyn$^{-/-}$ neurons yielded an average response of 0.39 ± 0.43 $\Delta F/F_0$, whereas WT average was 0.21 ± 0.19 $\Delta F/F_0$. Furthermore, an even higher increase of 100% was observed for the 1st-evoked Tomosyn$^{-/-}$ response in 2 Hz stimulation during which 36 WT and 48 Tomosyn$^{-/-}$ neurons showed active synaptic participation (**Figure 10a**, center). Active synapses responded with an average $\Delta F/F_0$ of 0.42 ± 0.35 for Tomosyn$^{-/-}$ and 0.21 ± 0.18 for WT. These findings suggest that initial stimulation of neuronal activity triggers increased synaptic response that has to be described by a mechanism apart from just increased participation rate. Interestingly, when 1st-evoked responses to 0.75 and 2 Hz are compared with mGT amplitude per genotype, WT synapses show similar $\Delta F/F_0$ throughout evoked and spontaneous activity (median $\Delta F/F_0$ in 0.75 Hz, 2 Hz and mGT were 0.15, 0.17 and 0.13, respectively; black signal traces in **Figure 10a**). However, Tomosyn$^{-/-}$ synapses show an increase in evoked *versus* spontaneous activity (median $\Delta F/F_0$ in 0.75 Hz, 2 Hz and mGT were 0.22, 0.32 and 0.14, respectively; blue signal traces in **Figure 10a**). Therefore, Tomosyn$^{-/-}$ neurons consistently showed evoked activity that was approximately two times the amplitude from both evoked WT response and spontaneous Tomosyn$^{-/-}$ events.

Results presented above were expanded by additional findings. I computed the average peak $\Delta F/F_0$ for every AP per neuron. I found that actively participating synapses in Tomosyn$^{-/-}$ neurons yield $\Delta F/F_0$ of 0.32 ± 0.26 as an average first response to 0.75 Hz stimulation (**Figure**

10c). The response was 68% higher than in active WT synapses which have an average $\Delta F/F_0$ of 0.19 ± 0.15. This difference was statistically significant which was not the case in subsequent APs in the 0.75 Hz train. Similarly, average $\Delta F/F_0$ in 2 Hz stimulation was 0.26 ± 0.22 for Tomosyn$^{-/-}$ and 0.17 ± 0.13 for WT (**Figure 10b**). Although this was statistically non-significant (p = 0.0872, Wilcoxon rank-sum), the increased effect of 53% is present. These results suggest that synaptic participation is not the sole reason for increased first response in Tomosyn$^{-/-}$ neurons.

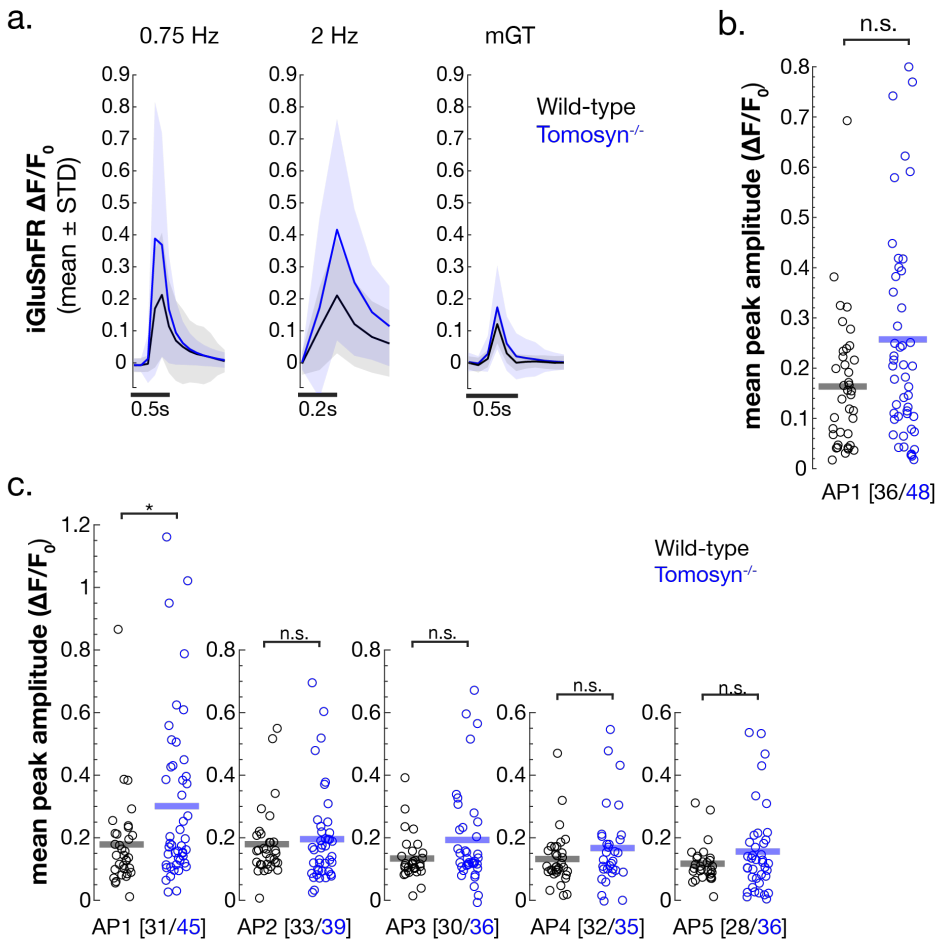

Figure 10. Analysis of the number of SVs released per actively participating synapse during evoked activity. (a) Average response shapes of first-evoked APs from only actively participating synapses during 0.75 (left) and 2 Hz (middle) stimulations (31 WT neurons, 2276 synapses; 45 Tomosyn$^{-/-}$ neurons, 5177 synapses). Average shapes of spontaneous mGT events per genotype (right; 200 WT events and 1739 Tomosyn$^{-/-}$ events). Black, WT; blue, Tomosyn$^{-/-}$. **(b)** Average peaks from active synapses per neuron for 1st-

evoked responses during 2 Hz. Black, 36 WT neurons; blue, 48 Tomosyn$^{-/-}$ neurons. Solid horizontal line, average. Wilcoxon rank-sum test ($p = 0.0872$). **(c)** Same as in (b) but for all 5 APs during 0.75 Hz stimulation. Numbers in squares, neurons with active synapses. Significance tested with Wilcoxon rank-sum test (n.s., not significant; * $p < 0.05$; ** $p < 0.01$; *** $p < 0.005$; **** $p < 0.001$)

4.3.3. SV pool dynamics disrupted in Tomosyn$^{-/-}$ synapses

Presynaptic compartment contains numerous synaptic vesicles for eventual release triggered by action potential (see Chapter 1.2.1). SVs are spatially organized in distinct vesicle pools which influence their release kinetics. Readily-releasable pool (RRP) contains fusion-ready SVs. High-frequency activity regimes induced, for instance, with high-frequency stimulation, are known to deplete RRP. This renders the synapse inactive until RRP is replenished during the recovery period. Because Tomosyn regulates SV cycling, I studied its effect on RRP depletion and subsequent replenishment during recovery. To accomplish this, I used a high-frequency stimulation paradigm during which neurons were stimulated with 100 APs at 40 Hz. Average response shape from all evoked activity after 40 Hz stimulation gave insight into (1) SV fusion or exocytosis rate, (2) combined SV exo- and endocytosis rate, and RRP replenishment (3) 1 and (4) 4 seconds post-RRP depletion (**Figure 11a**). Results show that RRP in WT synapses on average depleted after 4.85 ± 2.95 s. The same effect was reached significantly 53% faster in Tomosyn$^{-/-}$ synapses, after 2.30 ± 2.88 s (**Figure 11b**, left).

After an initial session of abrupt exocytosis, synapses continue with sustained SV fusion while recycling released vesicles to maintain activity competency. This period of combined exo- and endocytotic activity showed significantly different between Tomosyn$^{-/-}$ and WT synapses (**Figure 11b**, right). Based on the slope of average synaptic responses during 40 Hz stimulation, WT neurons would reach balance in exo-/endocytotic rate after 5.91 ± 16.46 s (39 neurons). This time was 82% longer for Tomosyn$^{-/-}$ synapses where balanced state would be achieved after 10.74 ± 3.67 s (49 neurons; $p < 0.001$, Wilcoxon rank-sum). To test whether this effect is influenced by potential disparities in probe decay times between genotypes, I analyzed the portion of the 40 Hz signal during which there are no 100 APs being delivered (part between 2nd and 3rd square in **Figure 11a**). Probe decay showed almost identical rates between genotypes (3.22 ± 1.11 s for WT and 3.07 ± 1.24 s for Tomosyn$^{-/-}$; **Figure 11c**).

Lastly, I studied synaptic recovery rates after sustained 40 Hz activity between genotypes. I looked at the peak prominence ratio between 1st recovery response (1 s after) and 1st-evoked response, as well as between 2nd recovery response (4 s after) and 1st-evoked response. Such ratios will show how far away are recovery amplitudes from reaching initial response strength (**Figure 11d**). Results show that average synaptic response in WT neurons 1 s after 40 Hz has peak-to-peak ratio of 0.51 ± 0.34, which increases after 4s to 0.60 ± 0.39. An increase suggests potential synaptic recovery; however, this change was not statistically significant. On the other hand, Tomosyn$^{-/-}$ synapses recover to 0.41 ± 0.28 of the initial peak response after 1 s, and to 0.47 ± 0.27 after 4 s of recovery. This increase was not significant. Tomosyn$^{-/-}$ increase was likewise smaller than in WT, and so were the time-locked ratios per recovery pulses between genotypes (i.e., 1s-to-1s and 4s-to-4s between Tomosyn$^{-/-}$ and WT).

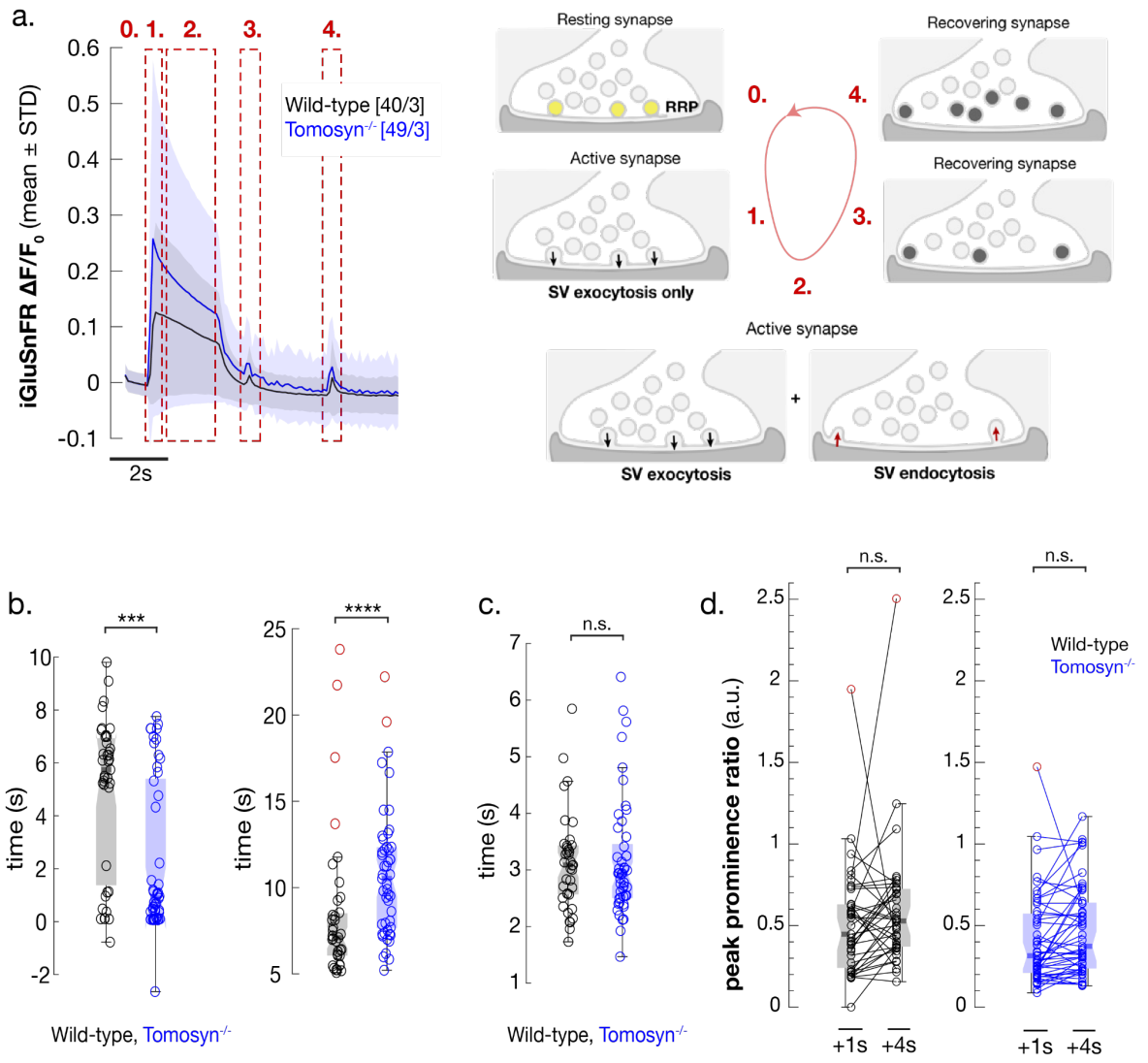

Figure 11. Comparison of synaptic vesicle pool dynamics between WT and Tomosyn$^{-/-}$ neurons after high-frequency stimulation. (a) Average WT and Tomosyn$^{-/-}$ synaptic responses to 100 APs at 40 Hz, with 2 subsequent recovery pulses. Solid line, mean; shade, STD. Dashed red squares: (1.) SV exocytosis rate, (2.) balance between exo- and endocytosis, synaptic recovery after (3.) 1 and (4.) 4 seconds. Squares (left) match illustrations (right). **(b)** Average RRP depletion time (left; black, 39 WT neurons; blue, 49 Tomosyn$^{-/-}$ neurons). Average time to reach a balanced exo-/endocytosis state (right). Red, outliers. **(c)** iGluSnFR probe's decay rate. Labels and neurons same as in (b). **(d)** Vesicle pool recovery 1 and 4 s after 40 Hz stimulation per genotype. Labels and neurons same as in (b). Significance tested with Wilcoxon rank-sum (n.s., not significant; * $p < 0.05$; ** $p < 0.01$; *** $p < 0.005$; **** $p < 0.001$).

5. DISCUSSION

This work thoroughly addressed the potential of iGluSnFR, a genetically encoded fluorescent reporter with affinity for glutamate, for application in studying functional connectivity of neuronal networks *in vitro* with single-synaptic resolution. The sufficient number of detected synapses and stable baseline expression, which was consistent throughout weeks of culturing, make iGluSnFR reliable for conducting optical experiments in cultures. iGluSnFR expressed in TTX-treated neurons confirmed dependency of vesicular release on stimulation-driven action potentials. The probe even allowed detection of stimulation-independent activity reflecting mGT events caused by spontaneous vesicle fusion. When neuronal activity was unrestricted, triggered synaptic responses yielded high iGluSnFR signal increase, detectable in individual synapses even after single stimulation trial. In genetically modified neurons lacking Tomosyn, iGluSnFR allowed quantitative description of altered presynaptic activity. These findings underlined critical benefits of using iGluSnFR for functional connectivity assessment.

In the past few decades, powerful optical tools have been developed to study functional relationships between co-active neurons in the network that have until now been mostly overlooked. Most common optical tools rely on reporting cytosolic calcium dynamics (**Grienberger & Konnerth**, **2012**). They approximate neuronal activity with somatic resolution. Ideally, however, functional connectivity should be studied by monitoring direct communication across many synapses in the network. Because synaptic communication is spatially confined, cytosolic calcium reporters underperform. When their localization is improved to target synapses (**Brockhaus et al.**, **2019**), temporal resolution of their signal is slow. Glutamate-sensing probes like iGluSnFR are steadily gaining traction for wide application in optical experiments (**Hao & Plested**, **2022**). This work has recognized the potential benefits of iGluSnFR for application in a network-wide context, so it aimed at systematically addressing its strengths and weaknesses.

Consistent with other studies (**Jensen et al.**, **2019**; **Vevea & Chapman**, **2020**), I found that iGluSnFR permits monitoring of glutamate release in multiple synaptic sites at once. Even in autaptic cultures like those used here, where one neuron is imaged per trial, iGluSnFR was successfully applied to screen activity of hundreds of synapses at once. The capacity for high-throughput readout makes iGluSnFR probe especially attractive *in vitro*, which standard

techniques do not provide. When designing iGluSnFR-based experiments, imaging just a few dozen cells generates sufficient data to capture both general and individual synaptic properties. Other benefits include cutting the experimental timeline and reducing the number of animals used. Although, concerns were raised that differences in iGluSnFR expression may be reflected in the fluorescence signal and therefore be misleading during signal interpretation (**Armbruster et al.**, **2020**). Higher expression leads to slower glutamate clearance from the synapse which in turn prolongs iGluSnFR signal, so Armbuster et al. (**2020**) suggest caution when comparing iGluSnFR-based findings from various brain regions. However, I used culturing protocols and experimental models consistently throughout the study, so it is unlikely that results presented here suffered from suggested expression-dependent effects in iGluSnFR signal. Nevertheless, I reported variability in iGluSnFR expression as the coefficient of variation in baseline fluorescence signal across synapses per neuron. This metric may benefit as future reference. Potentially better use of CoV calculation here would be correlating maximal increase in iGluSnFR signal per neuron with its F_0 CoV. Moreover, those correlations could be separated per culturing week to see whether significantly different outcomes in activity are detected.

In this study, I employed multiple stimulation frequencies to trigger various synaptic activity regimes for better understanding of the probe. Overall, iGluSnFR tracks individual synaptic activity with single-AP resolution across slow (0.75 Hz) and medium (2 Hz) stimulation frequencies, in both genetically altered and unaltered cell lines. Like in (**Parsons et al.**, **2016**) where they apply 100 Hz stimulations, faster synaptic responses to high-frequency 40 Hz stimulation used here were temporally merged into a continuous iGluSnFR signal. However, the signal accurately follows stimulation parameters like duration; therefore, individual AP responses can be easily deconvolved from the continuous signal. Temporal resolution of the signal would also benefit from employing faster image acquisition rate. Here I imaged iGluSnFR fluorescence at 10 Hz, which resulted in clustering of 4 APs in 1 frame. If imaged at 100 Hz for instance, 1 AP would span over multiple frames which potentially improve tracking single AP kinetics during high-frequency stimulation. Alternatively, newer iterations of iGluSnFR may perform better under high-frequency activity regimes (**Aggarwal et al.**, **2022**), and other competing glutamate reporters show promising performance in this regard (**Helassa et al.**, **2018**).

The main advantage of utilizing iGluSnFR *in vitro* is reaching single synaptic resolution. This study addressed another essential property of the probe, namely, its sensitivity to reflect altered synaptic activity. iGluSnFR was used before in concert with electrophysiological tools to quantify strong presynaptic phenotypes (**Vevea & Chapman**, **2020**). Here I examined how well the probe recapitulates electrophysiological findings related to more subtle changes in presynaptic activity. Electrophysiological recordings have so far been the main approach for characterization of neuronal activity *in vitro*. If iGluSnFR can demonstrate the same findings, the probe may be used instead, rather than next to standard tools. I used a knockout model of presynaptic protein Tomosyn because of its electrophysiologically well defined phenotype. Tomosyn-deficient neurons are known to respond with stronger fist-evoked amplitudes than WT, and have increased frequency of subthreshold activity (**Sauvola et al.**, **2021**). The Tomosyn-based model offered a two-fold advantage for current work. First, because there is a clear presynaptic phenotype, it should be undoubtedly apparent whether iGluSnFR can detect subtle alterations in presynaptic activity. Second, because Tomosyn-related knowledge comes predominantly from electrophysiological studies, using an advanced method like optical imaging of iGluSnFR allows discovering unique, yet uncharted insights related to Tomosyn's function in presynapse.

iGluSnFR reliably reported significantly increased first-evoked amplitude in Tomosyn$^{-/-}$ neurons compared to WT, both at the level of single synaptic traces and when averaged across all synapses per neuron. Level of increase varied across stimulation frequencies (183% for 0.75 Hz, 78% for 2 Hz, 100% for 40 Hz). These results are similar to what was found in hippocampal mossy fiber synapses in mice (85% increase in evoked EPSP amplitude) (**Sakisaka et al.**, **2008**), and neuromuscular junction in flies (142% increase in charge transfer in evoked excitatory junctional currents (eEJCs)) (**K. Chen et al.**, **2011**). However, increase levels reported here are higher than found in amplitude of fly eEJCs (61%) (**Sauvola et al.**, **2021**) and findings in worms (45% increase in evoked excitatory postsynaptic currents) (**McEwen et al.**, **2006**). Variance across reports may arise due to different synapse type, recording tools and stimulation frequencies used to trigger first-evoked response. Nevertheless, iGluSnFR evidently captures expected Tomosyn$^{-/-}$ phenotype in all tested conditions. The probe reported another compelling difference in synaptic response between genotypes. WT synapses often peaked 1 frame (100 ms) later than Tomosyn$^{-/-}$ synapses did. This suggests that Tomosyn-deficient synapses have faster response time. To explore this possibility, a good next step would

be comparing response rise times. Another option is increasing image acquisition rate from 10 Hz to 30 Hz or more, to enhance temporal resolution of the signal. This would result in more data points per AP shape; therefore, peak response times from different genotypes could be robustly examined.

iGluSnFR also allowed quantification of subthreshold activity per synapse rather than per neuron. This level of analysis is out of scope for most standard techniques, which are clueless to synaptic-level differences and can only quantify neuronal subthreshold activity recorded from soma. Like Soares et al. (**2017**) demonstrated by using iGluSnFR expressed in dendritic spines, glutamate uncaging over 25 min did not alter the amplitude of subthreshold responses in spines, although electrophysiological recording in the soma reported amplitude increase in somatic responses. In this study, I used iGluSnFR to address both amplitude and frequency of subthreshold events. Consistent with other results (**Sauvola et al.**, **2021**), I found more than a 500% increase in spontaneous glutamate release frequency in Tomosyn-deficient synapses, without significant change in peak amplitude compared to WT. Single synaptic resolution permits reporting fraction of spontaneously active synapses, which other studies do not report due to methodological shortcomings. I found that approximately 350% more Tomosyn$^{-/-}$ synapses exhibit spontaneous activity than in WT. Moreover, iGluSnFR showed there are differences in the fraction of synapses that participate during evoked activity as well. Tomosyn-deficient synapses participate with 97% increased rate during first-evoked response in 0.75 Hz stimulation, and with 40% higher rate during first-evoked in 2 Hz stimulation. These results suggest a causal relationship between synaptic participation and differences in evoked responses from Tomosyn$^{-/-}$ and WT neurons. A potential explanation lays in Tomosyn's role in synaptic vesicle cycle. Tomosyn inhibits SV priming (**Gracheva et al.**, **2006**; **McEwen et al.**, **2006**) and it regulates the size of readily releasable pool of SVs (**Cazares et al.**, **2016**). Therefore, Tomosyn-deficient synapses may have enhanced SV priming rate which increases the RRP size across all synapses. In turn, AP propagation from soma along neurites will result in higher synaptic participation because the probability of SV release is proportional to RRP size.

Interestingly, results from this work also suggested disrupted RRP dynamics in Tomosyn$^{-/-}$ synapses based on iGluSnFR signal. Tomosyn$^{-/-}$ synapses showed faster initial exocytosis rate and slower time to reach exo-/endocytosis balance during sustained stimulation.

Similar to above, a possible explanation is that lack of Tomosyn-based regulation of SV priming results in boosted exocytosis rate because many SVs have increased release probability. This would explain why RRP initially depletes faster in Tomosyn-deficient synapses. In turn, endocytotic mechanisms fail to keep up with boosted exocytosis, so exo-/endocytotic balance is reached only later. An alternative reason for disparity in exo-/endocytotic rates between genotypes might be faster decay in iGluSnFR signal in Tomosyn$^{-/-}$ synapses during 40 Hz stimulation. However, probe decay rates were compared and resulted with insignificant difference. Moreover, a potentially slower recovery rate after 40 Hz stimulation was proposed for Tomosyn$^{-/-}$ rather than WT synapses. However, differences in RRP dynamics and recovery suggested here need detailed attention. Results shown here can serve as starting point for future studies.

Lastly, an interesting result from iGluSnFR-based exploration of Tomosyn phenotype suggested that synaptic participation may not be the only mechanism behind differences in Tomosyn$^{-/-}$ and WT neuronal responses during 1st-evoked AP. When only active synapses were compared in amplitude, first-evoked Tomosyn$^{-/-}$ responses were 86% and 100% higher than WT (responses to 0.75 and 2 Hz, respectively). Moreover, the same Tomosyn$^{-/-}$ synapses have twice as strong first-evoked amplitude than seen in their spontaneous responses prior to stimulation, which was unaltered in case of WT synapses. However, interpretation of these results should be done with caution. Differences in only active synaptic responses may be due to multiple synapses being included in the 3-by-3 pixel region during image analysis. Then, Tomosyn synapses which are known to participate more, would produce higher average amplitude than average WT response, just like it was shown in this work. Nevertheless, another explanation is feasible. According to the quantal release hypothesis (Wang et al., 2019; Yu et al., 2011), there is a constant number of glutamate molecules stored in SVs. It is generally considered that spontaneous synaptic events represent fusion of a single SV per synapse. So, increase in evoked *versus* spontaneous iGluSnFR amplitude (and first-evoked Tomosyn$^{-/-}$ *versus* WT) implies higher glutamate concentration in synapse. It is attractive to speculate that, in absence of Tomosyn, an average presynapse potentially undergoes spontaneous fusion of multiple SVs during the first stimulation pulse. The other explanation includes larger SVs in Tomosyn-deficient presynapses or, in contrast to quantal hypothesis, more glutamate per SV. More research is needed to validate these findings. Wang et al. (2019) developed a method to quantify glutamate concentration per SV which may be used in this regard.

Taken all together, iGluSnFR showed excellent performance in endeavor to validate its credibility for quantitative studies *in vitro*. It replicated known findings from standard electrophysiological approaches, and it overcame their major limitations in that it reported altered activity from individual synapses. iGluSnFR showed potential beyond that, when utilized for discovery of yet unknown functional presynaptic properties behind detected alterations. To reduce ambiguity during iGluSnFR signal interpretation, however, more specific characterisation of the probe is still needed. For instance, is the probe prone to internalization during high-frequency stimulation? Does prolonged imaging decrease availability of the probe due to bleaching? Does iGluSnFR compete with endogenous glutamate receptors, and does their interaction affect signal intensity? Nevertheless, this work showed unprecedented potential for the probe to be considered in application to a more complex biological context, like in neural network-wide functional connectivity studies.

6. CONCLUSION

Glutamatergic synapses are attractive targets for uncovering the principles behind functionally connected neurons in the network. Novel glutamate-sensing fluorescent reporter iGluSnFR can be put to that use. This work showed:

1. Consistent expression and stability of fluorescence iGluSnFR signal in autaptic cultures. Increase in fluorescence reliably reflects glutamate release with single-synaptic resolution, both due to AP-triggered synaptic activity and spontaneous SV fusion below AP threshold.
2. The probe proved useful for reporting subtle changes in synaptic activity which have so far been addressed only on somatic level. iGluSnFR distinguished differences from genetically altered and unaltered synapses. Change in iGluSnFR intensity allowed precise quantification of evoked and subthreshold activity across distinct genotypes.
3. iGluSnFR gave insight into many response properties of individual synapses, like amplitude, participation rate, frequency of subthreshold events, and putatively pointed to different aspects of synaptic pool dynamics. These were successfully used to differentiate genetically altered synapses.

There are questions waiting to be answered using iGluSnFR, since its potential for network-wide research *in vitro* is undeniable.

7. REFERENCES

Adibi, M. (2019). Whisker-Mediated Touch System in Rodents: From Neuron to Behavior. *Frontiers in Systems Neuroscience*, *13*, 40. https://doi.org/10.3389/fnsys.2019.00040

Aggarwal, A., Liu, R., Chen, Y., Ralowicz, A. J., Bergerson, S. J., Tomaska, F., Hanson, T. L., Hasseman, J. P., Reep, D., Tsegaye, G., Yao, P., Ji, X., Kloos, M., Walpita, D., Patel, R., Mohr, M. A., Tilberg, P. W., Mohar, B., Team, T. G. P., … Podgorski, K. (2022). *Glutamate indicators with improved activation kinetics and localization for imaging synaptic transmission* (p. 2022.02.13.480251). bioRxiv. https://doi.org/10.1101/2022.02.13.480251

Ali, F., & Kwan, A. C. (2019). Interpreting in vivo calcium signals from neuronal cell bodies, axons, and dendrites: a review. *Neurophotonics*, *7*(01), 1. https://doi.org/10.1117/1.NPh.7.1.011402

Allen, C. B., Celikel, T., & Feldman, D. E. (2003). Long-term depression induced by sensory deprivation during cortical map plasticity in vivo. *Nature Neuroscience*, *6*(3), 291–299. https://doi.org/10.1038/nn1012

Andrade-Talavera, Y., & Rodríguez-Moreno, A. (2021). Synaptic Plasticity and Oscillations in Alzheimer's Disease: A Complex Picture of a Multifaceted Disease. *Frontiers in Molecular Neuroscience*, *14*, 696476. https://doi.org/10.3389/fnmol.2021.696476

Armbruster, M., Dulla, C. G., & Diamond, J. S. (2020). Effects of fluorescent glutamate indicators on neurotransmitter diffusion and uptake. *ELife*, *9*, 1–27. https://doi.org/10.7554/eLife.54441

Armbruster, M., Hanson, E., & Dulla, C. G. (2016). Glutamate clearance is locally modulated by presynaptic neuronal activity in the cerebral cortex. *Journal of Neuroscience*. https://doi.org/10.1523/JNEUROSCI.2066-16.2016

Aroniadou-Anderjaska, V., & Keller, A. (1995). LTP in the barrel cortex of adult rats. *Neuroreport*, *6*(17), 2297–2300. https://doi.org/10.1097/00001756-199511270-00007

Ashery, U., Bielopolski, N., Barak, B., & Yizhar, O. (2009). Friends and foes in synaptic transmission: the role of tomosyn in vesicle priming. *Trends in Neurosciences*. https://doi.org/10.1016/j.tins.2009.01.004

Barrett, D. G., Denève, S., & Machens, C. K. (2016). Optimal compensation for neuron loss. *ELife*, *5*, e12454. https://doi.org/10.7554/eLife.12454

Barroso-Flores, J., Herrera-Valdez, M. A., Galarraga, E., & Bargas, J. (2017). Models of Short-Term Synaptic Plasticity. In R. VonBernhardi, J. Eugenin, & K. J. Muller (Eds.), *Plastic Brain* (Vol. 1015, pp. 41–57). Springer International Publishing Ag. https://doi.org/10.1007/978-3-319-62817-2_3

Becherer, U., & Rettig, J. (2006). Vesicle pools, docking, priming, and release. *Cell and Tissue Research*, *326*(2), 393–407. https://doi.org/10.1007/s00441-006-0243-z

Benedetti, B. L., Glazewski, S., & Barth, A. L. (2009). Reliable and Precise Neuronal Firing during Sensory Plasticity in Superficial Layers of Primary Somatosensory Cortex. *Journal of Neuroscience*, *29*(38), 11817–11827. https://doi.org/10.1523/JNEUROSCI.3431-09.2009

Brockhaus, J., Brüggen, B., & Missler, M. (2019). Imaging and Analysis of Presynaptic Calcium Influx in Cultured Neurons Using synGCaMP6f. *Frontiers in Synaptic Neuroscience, 11.* https://www.frontiersin.org/articles/10.3389/fnsyn.2019.00012

Bronk, P., Deák, F., Wilson, M. C., Liu, X., Südhof, T. C., & Kavalali, E. T. (2007). Differential Effects of SNAP-25 Deletion on Ca^{2+} -Dependent and Ca^{2+} -Independent Neurotransmission. *Journal of Neurophysiology*, *98*(2), 794–806. https://doi.org/10.1152/jn.00226.2007

Broussard, G. J., Liang, R., & Tian, L. (2014). Monitoring activity in neural circuits with genetically encoded indicators. *Frontiers in Molecular Neuroscience*, *7*, 97. https://doi.org/10.3389/fnmol.2014.00097

Bullmore, E., & Sporns, O. (2009). Complex brain networks: Graph theoretical analysis of structural and functional systems. *Nature Reviews Neuroscience*. https://doi.org/10.1038/nrn2575

Buzsáki, G. (2010). Neural Syntax: Cell Assemblies, Synapsembles, and Readers. *Neuron*. https://doi.org/10.1016/j.neuron.2010.09.023

Cazares, V. A., Njus, M. M., Manly, A., Saldate, J. J., Subramani, A., Ben-Simon, Y., Sutton, M. A., Ashery, U., & Stuenkel, E. L. (2016). Dynamic Partitioning of Synaptic Vesicle Pools by the SNARE-Binding Protein Tomosyn. *The Journal of Neuroscience*, *36*(44), 11208–11222. https://doi.org/10.1523/JNEUROSCI.1297-16.2016

Celikel, T., Szostak, V. A., & Feldman, D. E. (2004). Modulation of spike timing by sensory deprivation during induction of cortical map plasticity. *Nature Neuroscience*, *7*(5), 534–541. https://doi.org/10.1038/nn1222

Chapman, E. R. (2008). How does synaptotagmin trigger neurotransmitter release? *Annual Review of Biochemistry*, *77*, 615–641. https://doi.org/10.1146/annurev.biochem.77.062005.101135

Chen, K., Richlitzki, A., Featherstone, D. E., Schwärzel, M., & Richmond, J. E. (2011). Tomosyn-dependent regulation of synaptic transmission is required for a late phase of associative odor memory. *Proceedings of the National Academy of Sciences of the United States of America*, *108*(45), 18482–18487. https://doi.org/10.1073/pnas.1110184108

Chen, T.-W., Wardill, T. J., Sun, Y., Pulver, S. R., Renninger, S. L., Baohan, A., Schreiter, E. R., Kerr, R. A., Orger, M. B., Jayaraman, V., Looger, L. L., Svoboda, K., & Kim, D. S. (2013). Ultrasensitive fluorescent proteins for imaging neuronal activity. *Nature*, *499*(7458), 295–300. https://doi.org/10.1038/nature12354

Chua, J. J. E. (2014). Macromolecular complexes at active zones: integrated nano-machineries for neurotransmitter release. *Cellular and Molecular Life Sciences : CMLS*. https://doi.org/10.1007/s00018-014-1657-5

Citri, A., & Malenka, R. C. (2008). Synaptic Plasticity: Multiple Forms, Functions, and Mechanisms. *Neuropsychopharmacology*, *33*(1), 18–41. https://doi.org/10.1038/sj.npp.1301559

Cui, Y., Liu, L. D., McFarland, J. M., Pack, C. C., & Butts, D. A. (2016). Inferring cortical variability from local field potentials. *Journal of Neuroscience*. https://doi.org/10.1523/JNEUROSCI.2502-15.2016

Dana, H., Sun, Y., Mohar, B., Hulse, B. K., Kerlin, A. M., Hasseman, J. P., Tsegaye, G., Tsang, A., Wong, A., Patel, R., Macklin, J. J., Chen, Y., Konnerth, A., Jayaraman, V., Looger, L. L., Schreiter, E. R., Svoboda, K., & Kim, D. S. (2019). High-performance calcium sensors for imaging activity in neuronal populations and microcompartments. *Nature Methods*, *16*(7), 649–657. https://doi.org/10.1038/s41592-019-0435-6

Dinstein, I., Heeger, D. J., & Behrmann, M. (2015). Neural variability: Friend or foe? *Trends in Cognitive Sciences*. https://doi.org/10.1016/j.tics.2015.04.005

Diril, M. K., Wienisch, M., Jung, N., Klingauf, J., & Haucke, V. (2006). Stonin 2 Is an AP-2-Dependent Endocytic Sorting Adaptor for Synaptotagmin Internalization and Recycling. *Developmental Cell*, *10*(2), 233–244. https://doi.org/10.1016/j.devcel.2005.12.011

Dreosti, E., & Lagnado, L. (2011). Optical reporters of synaptic activity in neural circuits. *Experimental Physiology*. https://doi.org/10.1113/expphysiol.2009.051953

Dreosti, E., Odermatt, B., Dorostkar, M. M., & Lagnado, L. (2009). A genetically encoded reporter of synaptic activity in vivo. *Nature Methods*, *6*(12), 883–889. https://doi.org/10.1038/nmeth.1399

Dubreuil, A., Valente, A., Beiran, M., Mastrogiuseppe, F., & Ostojic, S. (2022). The role of population structure in computations through neural dynamics. *Nature Neuroscience*, *25*(6), 783–794. https://doi.org/10.1038/s41593-022-01088-4

Eickhoff, S. B., & Müller, V. I. (2015). Functional Connectivity. In *Brain Mapping: An Encyclopedic Reference*. https://doi.org/10.1016/B978-0-12-397025-1.00212-8

Emperador-Melero, J., & Kaeser, P. S. (2020). Assembly of the presynaptic active zone. *Current Opinion in Neurobiology*. https://doi.org/10.1016/j.conb.2020.03.008

Farrant, M., & Nusser, Z. (2005). Variations on an inhibitory theme: phasic and tonic activation of GABAA receptors. *Nature Reviews Neuroscience*, *6*(3), 215–229. https://doi.org/10.1038/nrn1625

Fontanini, A., & Katz, D. B. (2008). Behavioral states, network states, and sensory response variability. *Journal of Neurophysiology*. https://doi.org/10.1152/jn.90592.2008

Gambino, F., Pagès, S., Kehayas, V., Baptista, D., Tatti, R., Carleton, A., & Holtmaat, A. (2014). Sensory-evoked LTP driven by dendritic plateau potentials in vivo. *Nature*. https://doi.org/10.1038/nature13664

Gracheva, E. O., Burdina, A. O., Holgado, A. M., Berthelot-Grosjean, M., Ackley, B. D., Hadwiger, G., Nonet, M. L., Weimer, R. M., & Richmond, J. E. (2006). Tomosyn inhibits synaptic vesicle priming in Caenorhabditis elegans. *Plos Biology*, *4*(8), 1426–1437. https://doi.org/10.1371/journal.pbio.0040261

Granseth, B., Odermatt, B., Royle, S. J., & Lagnado, L. (2006). Clathrin-Mediated Endocytosis Is the Dominant Mechanism of Vesicle Retrieval at Hippocampal Synapses. *Neuron*, *51*(6), 773–786. https://doi.org/10.1016/j.neuron.2006.08.029

Grienberger, C., & Konnerth, A. (2012). Imaging Calcium in Neurons. *Neuron*, *73*(5), 862–885. https://doi.org/10.1016/j.neuron.2012.02.011

Hao, Y., & Plested, A. J. R. (2022). Seeing glutamate at central synapses. *Journal of Neuroscience Methods*, *375*, 109531. https://doi.org/10.1016/j.jneumeth.2022.109531

Harada, K., Kamiya, T., & Tsuboi, T. (2016). Gliotransmitter release from astrocytes: functional, developmental and pathological implications in the brain. *Frontiers in Neuroscience*, *9*. https://www.frontiersin.org/articles/10.3389/fnins.2015.00499

Harris, K. D. (2005). Neural signatures of cell assembly organization. *Nature Reviews Neuroscience*, *6*(5), 399–407. https://doi.org/10.1038/nrn1669

Harris, K. M., & Weinberg, R. J. (2012). Ultrastructure of Synapses in the Mammalian Brain. *Cold Spring Harbor Perspectives in Biology*, *4*(5), a005587–a005587. https://doi.org/10.1101/cshperspect.a005587

He, G., Wang, X.-Y., Jia, Z., & Zhou, Z. (2022). Characterizing neurotrophic factor-induced synaptic growth in primary mouse neuronal cultures. *STAR Protocols*, *3*(1), 101112. https://doi.org/10.1016/j.xpro.2021.101112

Helassa, N., Dürst, C. D., Coates, C., Kerruth, S., Arif, U., Schulze, C., Simon Wiegert, J., Geeves, M., Oertner, T. G., & Török, K. (2018). Ultrafast glutamate sensors resolve high-frequency release at Schaffer collateral synapses. *Proceedings of the National Academy of Sciences of the United States of America*. https://doi.org/10.1073/pnas.1720648115

Hennig, M. H. (2013). Theoretical models of synaptic short term plasticity. *Frontiers in Computational Neuroscience*. https://doi.org/10.3389/fncom.2013.00045

Hires, S. A., Zhu, Y., & Tsien, R. Y. (2008). Optical measurement of synaptic glutamate spillover and reuptake by linker optimized glutamate-sensitive fluorescent reporters. *Proceedings of the National Academy of Sciences of the United States of America*. https://doi.org/10.1073/pnas.0712008105

Huang, C., Englitz, B., Reznik, A., Zeldenrust, F., & Celikel, T. (2020). *Information transfer and recovery for the sense of touch* [Preprint]. Neuroscience. https://doi.org/10.1101/2020.12.08.415729

Jaaskelainen, I. P., Ahveninen, J., Andermann, M. L., Belliveau, J. W., Raij, T., & Sams, M. (2011). Short-term plasticity as a neural mechanism supporting memory and attentional functions. *Brain Research*, *1422*, 66–81. https://doi.org/10.1016/j.brainres.2011.09.031

Jackson, R. E., & Burrone, J. (2016). Visualizing Presynaptic Calcium Dynamics and Vesicle Fusion with a Single Genetically Encoded Reporter at Individual Synapses. *Frontiers in Synaptic Neuroscience*, *8*. https://doi.org/10.3389/fnsyn.2016.00021

Jang, Y., Kim, S. R., & Lee, S. H. (2021). Methods of measuring presynaptic function with fluorescence probes. *Applied Microscopy*, *51*, 2. https://doi.org/10.1186/s42649-021-00051-0

Jensen, T. P., Zheng, K., Cole, N., Marvin, J. S., Looger, L. L., & Rusakov, D. A. (2019). Multiplex imaging relates quantal glutamate release to presynaptic Ca2+ homeostasis at

multiple synapses in situ. *Nature Communications*, *10*(1), 1414. https://doi.org/10.1038/s41467-019-09216-8

Keller, A. J., Dipoppa, M., Roth, M. M., Caudill, M. S., Ingrosso, A., Miller, K. D., & Scanziani, M. (2020). A Disinhibitory Circuit for Contextual Modulation in Primary Visual Cortex. *Neuron*, *108*(6), 1181-1193.e8. https://doi.org/10.1016/j.neuron.2020.11.013

Kennedy, M. B. (2000). Signal-processing machines at the postsynaptic density. *Science*. https://doi.org/10.1126/science.290.5492.750

Kerr, J. N. D., De Kock, C. P. J., Greenberg, D. S., Bruno, R. M., Sakmann, B., & Helmchen, F. (2007). Spatial organization of neuronal population responses in layer 2/3 of rat barrel cortex. *Journal of Neuroscience*, *27*(48), 13316–13328. https://doi.org/10.1523/JNEUROSCI.2210-07.2007

Koch, C., & Segev, I. (2000). The role of single neurons in information processing. *Nature Neuroscience*. https://doi.org/10.1038/81444

Laughlin, S. B., & Sejnowski, T. J. (2003). Communication in Neuronal Networks. *Science*, *301*(5641), 1870–1874. https://doi.org/10.1126/science.1089662

Liem, L. K., Simard, J. M., Song, Y., & Tewari, K. (1995). The Patch Clamp Technique. *Neurosurgery*, *36*(2), 382–392. https://doi.org/10.1227/00006123-199502000-00020

Malenka, R. C. (1995). LTP and LTD: Dynamic and Interactive Processes of Synaptic Plasticity. *The Neuroscientist*, *1*(1), 35–42. https://doi.org/10.1177/107385849500100106

Malenka, R. C., & Bear, M. F. (2004). LTP and LTD: an embarrassment of riches. *Neuron*, *44*(1), 5–21. https://doi.org/10.1016/j.neuron.2004.09.012

Marieb, E. N., & Hoehn, K. (2015). Human Anatomy & Physiology, Global Edition. In *Human Anatomy & Physiology*.

Marre, O., Amodei, D., Deshmukh, N., Sadeghi, K., Soo, F., Holy, T. E., & Berry, M. J. (2012). Mapping a Complete Neural Population in the Retina. *Journal of Neuroscience*, *32*(43), 14859–14873. https://doi.org/10.1523/JNEUROSCI.0723-12.2012

Marvin, J. S., Borghuis, B. G., Tian, L., Cichon, J., Harnett, M. T., Akerboom, J., Gordus, A., Renninger, S. L., Chen, T. W., Bargmann, C. I., Orger, M. B., Schreiter, E. R., Demb, J. B., Gan, W. B., Hires, S. A., & Looger, L. L. (2013). An optimized fluorescent probe for visualizing glutamate neurotransmission. *Nature Methods*, *10*(2), 162–170. https://doi.org/10.1038/nmeth.2333

Marvin, J. S., Scholl, B., Wilson, D. E., Podgorski, K., Kazemipour, A., Müller, J. A., Schoch, S., Quiroz, F. J. U., Rebola, N., Bao, H., Little, J. P., Tkachuk, A. N., Cai, E., Hantman, A. W., Wang, S. S. H., DePiero, V. J., Borghuis, B. G., Chapman, E. R., Dietrich, D., … Looger, L. L. (2018). Stability, affinity, and chromatic variants of the glutamate sensor iGluSnFR. *Nature Methods*, *15*(11), 936–939. https://doi.org/10.1038/s41592-018-0171-3

McEwen, J. M., Madison, J. M., Dybbs, M., & Kaplan, J. M. (2006). Antagonistic regulation of synaptic vesicle priming by tomosyn and UNC-13. *Neuron*, *51*(3), 303–315. https://doi.org/10.1016/j.neuron.2006.06.025

Meijer, M., Cijsouw, T., Toonen, R. F., & Verhage, M. (2015). Synaptic Effects of Munc18-1 Alternative Splicing in Excitatory Hippocampal Neurons. *PLoS ONE*, *10*(9), e0138950. https://doi.org/10.1371/journal.pone.0138950

Meijer, M., Rehbach, K., Brunner, J. W., Classen, J. A., Lammertse, H. C. A., van Linge, L. A., Schut, D., Krutenko, T., Hebisch, M., Cornelisse, L. N., Sullivan, P. F., Peitz, M., Toonen, R. F., Brüstle, O., & Verhage, M. (2019). A Single-Cell Model for Synaptic Transmission and Plasticity in Human iPSC-Derived Neurons. *Cell Reports*, *27*(7). https://doi.org/10.1016/j.celrep.2019.04.058

Mennerick, S., Que, J., Benz, A., & Zorumski, C. F. (1995). Passive and synaptic properties of hippocampal neurons grown in microcultures and in mass cultures. *Journal of Neurophysiology*, *73*(1), 320–332. https://doi.org/10.1152/jn.1995.73.1.320

Missler, M., Südhof, T. C., & Biederer, T. (2012). Synaptic cell adhesion. *Cold Spring Harbor Perspectives in Biology*. https://doi.org/10.1101/cshperspect.a005694

Mu, Y., & Poo, M. M. (2006). Spike timing-dependent LTP/LTD mediates visual experience-dependent plasticity in a developing retinotectal system. *Neuron*, *50*(1), 115–125. https://doi.org/10.1016/j.neuron.2006.03.009

O'Reilly, R. C. (2006). Biologically Based Computational Models of High-Level Cognition. *Science*, *314*(5796), 91–94. https://doi.org/10.1126/science.1127242

Ottersen, O. P., & Landsend, A. S. (1997). Organization of Glutamate Receptors at the Synapse. *European Journal of Neuroscience*, *9*(11), 2219–2224. https://doi.org/10.1111/j.1460-9568.1997.tb01640.x

Park, S., Bin, N.-R., Yu, B., Wong, R., Sitarska, E., Sugita, K., Ma, K., Xu, J., Tien, C.-W., Algouneh, A., Turlova, E., Wang, S., Siriya, P., Shahid, W., Kalia, L., Feng, Z.-P., Monnier, P. P., Sun, H.-S., Zhen, M., … Sugita, S. (2017). UNC-18 and Tomosyn Antagonistically Control Synaptic Vesicle Priming Downstream of UNC-13 in Caenorhabditis elegans. *Journal of Neuroscience*, *37*(36), 8797–8815. https://doi.org/10.1523/JNEUROSCI.0338-17.2017

Parsons, M. P., Vanni, M. P., Woodard, C. L., Kang, R., Murphy, T. H., & Raymond, L. A. (2016). Real-time imaging of glutamate clearance reveals normal striatal uptake in Huntington disease mouse models. *Nature Communications*, *7*. https://doi.org/10.1038/ncomms11251

Peng, Y., Mittermaier, F. X., Planert, H., Schneider, U. C., Alle, H., & Geiger, J. R. P. (2019). High-throughput microcircuit analysis of individual human brains through next-generation multineuron patch-clamp. *ELife*, *8*, e48178. https://doi.org/10.7554/eLife.48178

Purves, D., Augustine, G. J., Fitzpatrick, D., Hall, W. C., LaMantia, A.-S., McNamara, J. O., & White, L. E. (2008). Neuroscience (6th ed.). In *Textbook/Study Guide*.

Ranjbar-Slamloo, Y., & Arabzadeh, E. (2019). Diverse tuning underlies sparse activity in layer 2/3 vibrissal cortex of awake mice. *The Journal of Physiology*, *597*(10), 2803–2817. https://doi.org/10.1113/JP277506

Razlivanov, I., Liew, T., Moore, E. W., Al-Kathiri, A., Bartram, T., Kuvshinov, D., & Nikolaev, A. (2018). Long-term imaging of calcium dynamics using genetically encoded calcium indicators and automatic tracking of cultured cells. *BioTechniques*, *65*(1), 37–39. https://doi.org/10.2144/btn-2018-0024

Rossini, P. M., Di Iorio, R., Bentivoglio, M., Bertini, G., Ferreri, F., Gerloff, C., Ilmoniemi, R. J., Miraglia, F., Nitsche, M. A., Pestilli, F., Rosanova, M., Shirota, Y., Tesoriero, C., Ugawa, Y., Vecchio, F., Ziemann, U., & Hallett, M. (2019). Methods for analysis of brain connectivity: An IFCN-sponsored review. *Clinical Neurophysiology*, *130*(10), 1833–1858. https://doi.org/10.1016/j.clinph.2019.06.006

Sabatini, B. L., & Tian, L. (2020). Imaging Neurotransmitter and Neuromodulator Dynamics In Vivo with Genetically Encoded Indicators. *Neuron*, *108*(1), 17–32. https://doi.org/10.1016/j.neuron.2020.09.036

Sadakane, O., Masamizu, Y., Watakabe, A., Terada, S.-I., Ohtsuka, M., Takaji, M., Mizukami, H., Ozawa, K., Kawasaki, H., Matsuzaki, M., & Yamamori, T. (2015). Long-Term Two-Photon Calcium Imaging of Neuronal Populations with Subcellular Resolution in Adult Non-human Primates. *Cell Reports*, *13*(9), 1989–1999. https://doi.org/10.1016/j.celrep.2015.10.050

Saheki, Y., & De Camilli, P. (2012). Synaptic Vesicle Endocytosis. *Cold Spring Harbor Perspectives in Biology*, *4*(9), a005645. https://doi.org/10.1101/cshperspect.a005645

Saitsu, H., Kato, M., Mizuguchi, T., Hamada, K., Osaka, H., Tohyama, J., Uruno, K., Kumada, S., Nishiyama, K., Nishimura, A., Okada, I., Yoshimura, Y., Hirai, S. I., Kumada, T., Hayasaka, K., Fukuda, A., Ogata, K., & Matsumoto, N. (2008). De novo mutations in the gene encoding STXBP1 (MUNC18-1) cause early infantile epileptic encephalopathy. *Nature Genetics*, *40*(6). https://doi.org/10.1038/ng.150

Sakisaka, T., Yamamoto, Y., Mochida, S., Nakamura, M., Nishikawa, K., Ishizaki, H., Okamoto-Tanaka, M., Miyoshi, J., Fujiyoshi, Y., Manabe, T., & Takai, Y. (2008). Dual

inhibition of SNARE complex formation by tomosyn ensures controlled neurotransmitter release. *Journal of Cell Biology*, *183*(2), 323–337. https://doi.org/10.1083/jcb.200805150

Sankaranarayanan, S., De Angelis, D., Rothman, J. E., & Ryan, T. A. (2000). The use of pHluorins for optical measurements of presynaptic activity. *Biophysical Journal*, *79*(4), 2199–2208. https://doi.org/10.1016/S0006-3495(00)76468-X

Sauvola, C. W., Akbergenova, Y., Cunningham, K. L., Aponte-Santiago, N. A., & Littleton, J. T. (2021). The decoy SNARE Tomosyn sets tonic versus phasic release properties and is required for homeostatic synaptic plasticity. *ELife*, *10*, e72841. https://doi.org/10.7554/eLife.72841

Shen, Y., Nasu, Y., Shkolnikov, I., Kim, A., & Campbell, R. E. (2020). Engineering genetically encoded fluorescent indicators for imaging of neuronal activity: Progress and prospects. *Neuroscience Research*, *152*, 3–14. https://doi.org/10.1016/j.neures.2020.01.011

Soares, C., Lee, K. F. H., & Béïque, J. C. (2017). Metaplasticity at CA1 Synapses by Homeostatic Control of Presynaptic Release Dynamics. *Cell Reports*, *21*(5), 1293–1303. https://doi.org/10.1016/j.celrep.2017.10.025

Spinal Reflex Electrophysiology. (n.d.). Retrieved September 2, 2022, from http://humanphysiology.academy/Neurosciences%202015/Chapter%202/P.2.2b%20Spinal%20Reflex%20Electrophysiology.html

Stamberger, H., Nikanorova, M., Willemsen, M. H., Accorsi, P., Angriman, M., Baier, H., Benkel-Herrenbrueck, I., Benoit, V., Budetta, M., Caliebe, A., Cantalupo, G., Capovilla, G., Casara, G., Courage, C., Deprez, M., Destrée, A., Dilena, R., Erasmus, C. E., Fannemel, M., … Weckhuysen, S. (2016). STXBP1 encephalopathy: A neurodevelopmental disorder including epilepsy. *Neurology*.

Südhof, T. C. (1995). The synaptic vesicle cycle: A cascade of protein-protein interactions. *Nature*. https://doi.org/10.1038/375645a0

Südhof, T. C. (2004). The synaptic vesicle cycle. *Annual Review of Neuroscience*. https://doi.org/10.1146/annurev.neuro.26.041002.131412

Südhof, T. C. (2012). The presynaptic active zone. *Neuron*. https://doi.org/10.1016/j.neuron.2012.06.012

Südhof, T. C., & Rizo, J. (2011). Synaptic vesicle exocytosis. *Cold Spring Harbor Perspectives in Biology*. https://doi.org/10.1101/cshperspect.a005637

Sudlow, A. W., McFerran, B. W., Bodill, H., Barnard, R. J. O., Morgan, A., & Burgoyne, R. D. (1996). Similar effects of α- and β-SNAP on Ca^{2+} -regulated exocytosis. *FEBS Letters*, *393*(2–3), 185–188. https://doi.org/10.1016/0014-5793(96)00880-0

Tian, L., Hires, S. A., & Looger, L. L. (2012). Imaging Neuronal Activity with Genetically Encoded Calcium Indicators. *Cold Spring Harbor Protocols*, *2012*(6), pdb.top069609. https://doi.org/10.1101/pdb.top069609

Toonen, R. F. G., & Verhage, M. (2007). Munc18-1 in secretion: lonely Munc joins SNARE team and takes control. *Trends in Neurosciences*. https://doi.org/10.1016/j.tins.2007.08.008

van Brakel, J. P. G. (2020). *Robust peak detection algorithm using z-scores* (Version 2020-11-08). Stack Overflow. https://stackoverflow.com/questions/22583391/peak-signal-detection-in-realtime-timeseries-data/22640362#22640362

Vardar, G., Chang, S., Arancillo, M., Wu, Y.-J., Trimbuch, T., & Rosenmund, C. (2016). Distinct Functions of Syntaxin-1 in Neuronal Maintenance, Synaptic Vesicle Docking, and Fusion in Mouse Neurons. *Journal of Neuroscience*, *36*(30), 7911–7924. https://doi.org/10.1523/JNEUROSCI.1314-16.2016

Verhage, M., Maia, A. S., Plomp, J. J., Brussaard, A. B., Heeroma, J. H., Vermeer, H., Toonen, R. F., Hammer, R. E., Van Den Berg, T. K., Missler, M., Geuze, H. J., & Südhof, T. C. (2000). Synaptic assembly of the brain in the absence of neurotransmitter secretion. *Science*, *287*(5454). https://doi.org/10.1126/science.287.5454.864

Vevea, J. D., & Chapman, E. R. (2020). Acute disruption of the synaptic vesicle membrane protein synaptotagmin 1 using knockoff in mouse hippocampal neurons. *ELife*, *9*, 1–24. https://doi.org/10.7554/eLife.56469

Wang, Y., Fathali, H., Mishra, D., Olsson, T., Keighron, J. D., Skibicka, K. P., & Cans, A.-S. (2019). Counting the Number of Glutamate Molecules in Single Synaptic Vesicles. *Journal of the American Chemical Society*, *141*(44), 17507–17511. https://doi.org/10.1021/jacs.9b09414

Wilent, W. B., & Contreras, D. (2005). Stimulus-Dependent Changes in Spike Threshold Enhance Feature Selectivity in Rat Barrel Cortex Neurons. *Journal of Neuroscience*, *25*(11), 2983–2991. https://doi.org/10.1523/JNEUROSCI.4906-04.2005

Wollmuth, L. P. (2018). Ion permeation in ionotropic glutamate receptors: still dynamic after all these years. *Current Opinion in Physiology*, *2*, 36–41. https://doi.org/10.1016/j.cophys.2017.12.003

Xie, Y., Chan, A. W., McGirr, A., Xue, S., Xiao, D., Zeng, H., & Murphy, T. H. (2016). Resolution of High-Frequency Mesoscale Intracortical Maps Using the Genetically Encoded Glutamate Sensor iGluSnFR. *Journal of Neuroscience*, *36*(4), 1261–1272. https://doi.org/10.1523/JNEUROSCI.2744-15.2016

Yizhar, O., & Ashery, U. (2008). Modulating Vesicle Priming Reveals that Vesicle Immobilization Is Necessary but not Sufficient for Fusion-Competence. *Plos One*, *3*(7), e2694. https://doi.org/10.1371/journal.pone.0002694

Yu, J., Qian, H., Chen, N., & Wang, J.-H. (2011). Quantal Glutamate Release Is Essential for Reliable Neuronal Encodings in Cerebral Networks. *PLoS ONE*, *6*(9), e25219. https://doi.org/10.1371/journal.pone.0025219

Yuste, R. (2015). From the neuron doctrine to neural networks. *Nature Reviews Neuroscience*. https://doi.org/10.1038/nrn3962

Zhang, Y., Rózsa, M., Bushey, D., Jihong Zheng, Reep, D., Yajie Liang, Broussard, G. J., Tsang, A., Getahun Tsegaye, Patel, R., Sujatha Narayan, Lim, J. X., Rongwei Zhang, Ahrens, M. B., Turner, G. C., Wang, S. S.-H., Svoboda, K., Korff, W., Schreiter, E. R.,

… Looger, L. L. (2020). *jGCaMP8 Fast Genetically Encoded Calcium Indicators*. 361685 Bytes. https://doi.org/10.25378/JANELIA.13148243

Zhao, C., Slevin, J. T., & Whiteheart, S. W. (2007). Cellular functions of NSF: Not just SNAPs and SNAREs. *FEBS Letters*, *581*(11), 2140–2149. https://doi.org/10.1016/j.febslet.2007.03.032

8. CURRICULUM VITAE

I was born in 1995 in Strahoninec, a small place near Čakovec in Međimurje County, Croatia. I attended a general grammar school programme in Gymnasium Josip Slavenski in Čakovec from 2010 to 2014, where I obtained a high school degree. In 2014, I enrolled for a bachelor's programme in General biology at Faculty of Science, University of Zagreb, Croatia. I obtained my BSc degree in 2017, immediately after which I enrolled for a master's programme in Experimental biology at Faculty of Science, University of Zagreb, where I chose to specialize in Physiology and immunobiology. I finished all compulsory master's courses during my first year, but I did not continue into my second year in 2018. Instead, I was accepted into a second master's programme in Medical biology at Radboud University, Nijmegen, The Netherlands, where I specialized in Neurobiology. I obtained my MSc degree in Medical biology in 2021. Shortly prior to graduating from Radboud University, in 2020 I returned to University of Zagreb to finalize the second year of the master's programme in Experimental biology. Before graduating from University of Zagreb, I got a PhD position in the Zeldenrust/Celikel lab in the Neurophysics section at Donders Centre for Neuroscience, Radboud University, Nijmegen, The Netherlands.

I was part of several organizing committees, a student association and I contributed to a student magazine during my studies at University of Zagreb. I attended summer schools and symposia outside of the general study curriculum. I was awarded Rector's award for socially useful work in the academic and wider community at University of Zagreb.